AIAA JOURNAL
Vol. 47, No. 1, January 2009

# Efficient Mode-Based Computational Approach for Jointed Structures: Joint Interface Modes

Wolfgang Witteveen*
*Linz Center of Mechatronics, 4040 Linz, Austria*
and
Hans Irschik†
*Johannes Kepler University, 4040 Linz, Austria*

DOI: 10.2514/1.38436

**The mechanical response of complex elastic structures that are assembled of substructures is significantly influenced by joints such as bolted joints, spot-welded seams, adhesive-glued joints, and others. In this respect, computational techniques, which are based on the direct finite element method or on classical modal reduction procedures, unfortunately show an inefficient balance between computation time and accuracy. In the present paper, a novel reduction method for the physical (nodal) joint interface degrees of freedom is presented, which we call joint interface modes. For the computation of the joint interface modes, Newton's third law (principle of equivalence of forces) across the joint is explicitly accounted for the mode generation. This leads to a dimension of the generalized joint interface degrees of freedom in the reduced system, which is a factor of 2 or more smaller than in conventional reduction methods, which do not consider Newton's third law. Two different approaches for the computation of the joint interface modes are presented. Numerical studies with bolted joints of different complexities are performed using a simple but representative constitutive joint model. It is demonstrated that the new joint-interface-mode formulation leads to both excellent accuracy and high computational efficiency.**

## Nomenclature

| | | |
|---|---|---|
| $d$ | = | viscous damping coefficient |
| $\mathbf{f}$ | = | vector of physical forces |
| $\tilde{\mathbf{G}}$, ${}_{\#}\tilde{\mathbf{G}}$ | = | transformation matrices |
| $\tilde{\mathbf{H}}$, ${}_{\#}\tilde{\mathbf{H}}$ | = | transformation matrices |
| $\tilde{\mathbf{I}}$ | = | identity matrix |
| $\tilde{\mathbf{K}}$ | = | stiffness matrix |
| $\tilde{\mathbf{M}}$ | = | mass matrix |
| $\mathbf{n}$ | = | total number of degrees of freedom |
| $\mathbf{n}_{\mathrm{B}}$ | = | number of boundary degrees of freedom |
| $\mathbf{n}_{\mathrm{C}}$ | = | number of modes |
| $\mathbf{n}_{\mathrm{I}}$ | = | number of inner degrees of freedom |
| $\mathbf{n}_{I\setminus\mathrm{IJ}}$ | = | number of inner degrees of freedom without joint degrees of freedom |
| $\mathbf{n}_{\mathrm{IJ}}$ | = | number of joint degrees of freedom |
| $\mathbf{n}_{\mathrm{R}}$ | = | number of considered modes |
| $p$ | = | index of the vector norm |
| $\tilde{\mathbf{Q}}$ | = | rotation matrix |
| $\mathbf{q}$ | = | vector of generalized coordinates |
| $\tilde{\mathbf{R}}$ | = | transformation matrix |
| $\mathbf{t}$ | = | surface force |
| $\mathbf{x}$ | = | vector of displacements in physical coordinates (for example, finite element degrees of freedom) |
| $\alpha$ | = | relative error |
| $\Delta\mathbf{x}$ | = | vector of relative displacements |
| $\boldsymbol{\sigma}$ | = | vector of stresses (e.g., von Mises) |
| $\tilde{\boldsymbol{\Phi}}$ | = | matrix of modes (modal transformation matrix) |
| $\boldsymbol{\varphi}$ | = | trial vector (commonly called mode) |
| $\tilde{\boldsymbol{\Omega}}$ | = | diagonal matrix of eigenvalues |

*Subscripts*

| | | |
|---|---|---|
| $B$ | = | boundary degrees of freedom |
| $I$ | = | inner degrees of freedom |
| IJ | = | joint interface degrees of freedom |
| $I\setminus$IJ | = | inner degrees of freedom without joint interface degrees of freedom |
| $i$ | = | index of the joint surface |
| $i$ | = | index of the finite element body |
| red | = | quantity in the reduced system |
| trans | = | transformed into modal space |

*Superscripts*

| | | |
|---|---|---|
| IJ | = | quantity expressed in the joint coordinate system |
| LBRF | = | quantity expressed in the local-body reference frame |
| $m$ | = | mode-based solution |
| $r$ | = | reference solution |
| red | = | quantity in the reduced system |
| SFRF | = | quantity expressed in the space-fixed reference frame |
| $T$ | = | transpose of a matrix |
| $-1$ | = | inverse of a matrix |
| $*$ | = | unstressed reference position |
| $*$ | = | full matrix of modes (full solution of according eigenvalue problem) |

## I. Introduction

THE global stiffness and damping properties of a metallic structure that consists of jointed substructures are strongly influenced by the local characteristics of the involved joints such as bolted joints, spot-welded seams, adhesive-glued joints, and others. The global stiffness and damping depend nonlinearly on the joint pressure distribution, and the latter depends nonlinearly on the system state. The global damping that is introduced by joints of this kind is usually higher than a factor of 10 in comparison with material damping. In addition to stiffness and mass properties, the presence of joints thus represents the most important factor for the realistic vibration analysis of such structures. For an extensive report on constitutive modeling of the mechanical behavior of joints, see, for example, the review by Gaul and Nitsche [1].

Received 7 May 2008; revision received 9 July 2008; accepted for publication 9 July 2008. 

*Senior Researcher, Multi-Body and Multi-Field Dynamics; wolfgang.witteveen@lcm.at.

†Professor and Head, Institute of Technical Mechanics; irschik@mechatronik.uni-linz.ac.at. Member AIAA.

In engineering practice, jointed structural systems are usually analyzed by means of commercial finite element (FE) codes. The strength of these FE codes is the static solution of FE structures with a considerably high number of degrees of freedom (DOF), up to several millions. Because of this huge number of DOF, the time integration of the dynamic behavior of jointed structures so far is economically not possible without problem-oriented restrictions, such as in the size of the FE model (the number of DOF), the number of time integration points, or the fact that inertia effects cannot be considered (quasi-static instead of full dynamic simulation).

Time integration of linear elastic structures without nonlinear joints can be effectively and consistently performed by the modal approach; that is, by a linear combination of time-invariant Ritz-type deformation shapes, commonly called *modes*. The modal approach reduces the number of DOF of linear FE structures, so that time integration is possible without significant loss of accuracy (within a well-defined frequency band). A wide variety of modal reduction methods with different characteristics and advantages have been presented during the last decades; for example, a review of reduction methods has been published by Noor [2]. Different component mode synthesis (CMS) methods have been reviewed by, among others, Craig [3,4] and Meirovitch [5]. The recently published book of Zu [6] has given an exhaustive overview on the issue of model reduction from its beginning in the 1960s until the turn of the millennium. A comprehensive numerical comparison study has been performed by Koutsovasilis and Beitelschmidt [7] for an elastic piston rod. The latter publication includes the classical reduction methods such as CMS as well as more recently developed methods such as the improved reduction system method, system equivalent reduction expansion process, or Krylov-subspace methods (see [6,7] for a detailed reference).

Many reduction methods do preserve the nodal degrees of freedom at interfaces. The interface is defined as the domain (or DOF) on which external forces may act. Examples are the well known Guyan [8] reduction, the CMS method proposed by Hurty [9], or the famous and widely used Craig–Bampton [10] CMS. In these formulations, each interface DOF leads to a so-called constraint mode in the final mode base. For an accurate and local application of contact and friction laws in a joint, the nodal DOF of a contact surface need to be considered as an interface. This leads to an inefficient number of modes in the cases of the huge FE models and large interfaces that are typical for industrial applications, particularly in aero- and astronautics.

Some approaches do not take the interface into account at all, such as some Krylov-subspace methods (e.g., [11]). Other reduction methods do not explicitly preserve the nodal DOF of the joint. The physical interface DOF are then replaced by generalized DOF. Examples are the interface modes that are a generalization of the latter-mentioned constraint modes (see, for example, Castanier et al. [12], Tran [13], Farhat and Geradin [14], or Balmes [15]). The approximation of the interface deformation by a proper set of interface modes instead of all constraint modes will lead to a significant reduction of DOF, associated with an acceptable accuracy of the result. However, the remaining number of interface modes may still be considerably high and, in the case of complex interfaces, can dominate the dimension of the entire mode base.

Some approaches in the past suggested the consideration of the contact and friction directly in the mode base. Muravyov and Hutton [16] suggested an extension of the CMS to systems with a nonzero viscous damping matrix. This method leads to complex eigenvectors and eigenvalues and can capture the locality of the phenomenon but cannot represent its nonlinearity and an energy dissipation, which has just a weak frequency dependency (Gaul and Nitsche [1]). Nonlinear modes, which are suggested by Rosenberg [17], may capture the nonlinearities, but the implication of updating the modes and eigenvalues during simulation makes this approach impractical for large FE models in industrial engineering practice.

To the best knowledge of the present authors, all reduction methods in the literature have in common that mechanical-joint characteristics are not considered for the computation of real and time-invariant mode shapes, but are enforced at the stage of mode-based time integration only. It is certainly desirable, however, to have a method at disposal that is able to consider at least Newton's third law across the joint interface at the stage of mode generation, before time integration starts. Therefore, a problem-oriented extension to existing mode bases, which we denote as joint interface modes (JIMs), will be derived in Sec. III. Joint interface modes are characterized by the consideration of Newton's third law across the joint that is already at the stage of mode generation. Using JIMs instead of the aforementioned interface modes leads to a significant smaller mode base that is capable of representing the dynamic behavior of structures with nonlinear joints (see Sec. IV).

Note that modeling contact and friction is not part of the computation of JIMs. The purpose of the JIMs is to provide as few interface DOF as possible and as many interface DOF as necessary to apply realistic contact and friction forces on the interfaces during the mode-based time integration.

The work in the present paper is organized as follows:

1) Because our method is intended to also be used in connection with flexible multibody dynamic systems, some kinematical considerations on modally represented jointed structures in the context of the floating-frame-of-reference formulation (FFRF) (see Shabana [18]) are performed in the next section. In a mode-based computation, a jointed structure can be represented either by a single mode base of the entire structure or by two mode bases of the separate substructures. Both approaches are equivalent in terms of accuracy, but there is a remarkable difference with respect to the computational effort, due to the fact that time-dependent matrices need to be updated in the case of two separate flexible bodies.

2) In Sec. III, the novel concept of JIMs is presented. Based on the local continuity of forces acting on the two surfaces that are connected by the joint, two suitable static reduction methods are introduced to compute the JIMs as an extension to existing mode bases. One reduction technique is based on the full equation of motion, and the other reduction is based on a Guyan-type [8] reduced equation of motion. The correlation of both mode bases is subsequently demonstrated by means of a simple beam example.

3) In the last section, the accuracy of the proposed method is demonstrated by means of numerical examples in which it is shown that the proposed JIMs are able to reach the computational efficiency of the modal approach and the accuracy of a full FE computation.

A preliminary version of this work has been published in [19].

## II. Kinematical Considerations in the Context of a Floating-Frame-of-Reference Formulation

There are two main possibilities to model a jointed structure in the framework of a mode-based computation:

1) Each substructure is represented by its own flexible body and consequently by its own mode base. The connecting elements of the substructures, such as bolts, screws, spot welds, etc., are not part of the mode base and need to be modeled separately.

2) The entire structure is represented as a single flexible body that leads to a single mode base. Consequently, the connection elements are part of the FE model and part of the mode base. The faces in contact are congruent free faces.

Both approaches have in common that the contact forces are applied as external forces. Both possibilities are equivalent concerning the results, but there is a huge difference in terms of computational effort if the modes are used as trial vectors in the framework of a FFRF, as will be shown subsequently.

### A. Model with Two Separate Flexible Substructures

Figure 1 shows two deformable bodies. Each body of Fig. 1 has a local-body reference frame (LBRF) and its own mode base. It is assumed that the flexible bodies are modeled by the FE method. In the final assembly, both bodies are connected via a common interface: the joint. The area connecting the two jointed bodies will be subsequently denoted as the joint or joint interface. This interface is taken to be prescribed and the relative displacements of the involved joint surfaces are taken as small. These conditions are valid

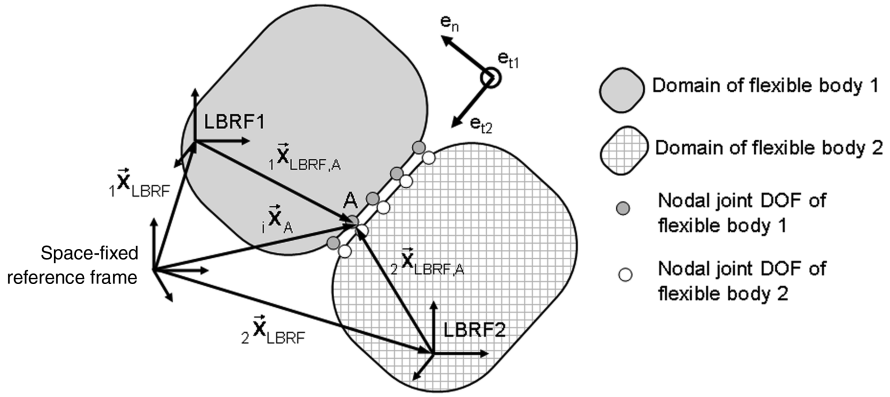


**Fig. 1 Two deformable bodies with a common interface (joint).**

for many technical interfaces such as bolted joints, press fits, adhesive joints, spot-welded seams, and others.

The $(3 \times 1)$ current position vector of the LBRF of the $i$th body $(i = 1, 2)$ expressed in the space-fixed reference frame (SFRF) is denoted as ${}_i\mathbf{x}_{\mathrm{LBRF}}$ in Fig. 1. In the FE method, the flexibility of the entire joint is modeled by nodal DOF. The nodes corresponding to the joint are indicated in Fig. 1 by dots and the other nodal DOF of the structure are omitted in Fig. 1. To collect all position vectors of all FE nodes that are part of the joint, the vector ${}_i\mathbf{x}_{\mathrm{IJ}}$ is introduced. The number of all nodal DOF of the flexible bodies 1 and 2 that belong to the joint is $\mathbf{n}_{\mathrm{IJ}}$. In the 3-D case, $\mathbf{n}_{\mathrm{IJ}}$ is 3 times the number of the involved nodes. For the sake of simplicity, it is assumed that all FE nodes of flexible body 1 that belong to the common joint interface have a unique counterpart that belongs to flexible body 2. Initially, however, the position vectors of the nodes at the interface do coincide so that

$$ {}_1\mathbf{x}^*_{\mathrm{IJ}} = {}_2\mathbf{x}^*_{\mathrm{IJ}} \tag{1} $$

The superscript $*$ denotes the initial state. In addition to the unstressed initial state and when the joint is not sticking, Eq. (1) will not hold. Furthermore, Eq. (1) requires that the dimension of ${}_i\mathbf{x}_{\mathrm{IJ}}$ has to be $(\mathbf{n}_{\mathrm{IJ}}/2 \times 1)$. Note that for the sake of clarity, the joint nodes in Fig. 1 are not indicated as coincident, although they are.

Because this section is dedicated to kinematical investigations, the dynamic interaction between the joint surfaces is not of particular interest yet. One may imagine that there is a contact law acting between ${}_1\mathbf{x}_{\mathrm{IJ}}$ and ${}_2\mathbf{x}_{\mathrm{IJ}}$.

In many practical applications, joints do have a special orientation (e.g., flat surfaces, cylindrical surfaces, etc.). Therefore, the motion normal and tangential to the contact area is of special interest. A transformation into a joint-oriented coordinate system is beneficial. This joint coordinate system is indicated in Fig. 1 with the unity vectors $\mathbf{e}_n$, $\mathbf{e}_{t1}$, and $\mathbf{e}_{t2}$ and is moving with one of the two flexible bodies' local reference frame. For a plane contact, the choice of a Cartesian coordinate system seems to be advantageous, but in the case of other contacts (e.g., press fit with cylindrical surfaces), other coordinate systems may be more beneficial.

The deformation of each body is described with respect to its LBRF. The total deformation is a combination of the rigid-body motion of the LBRF and the elastic deformation of the body's material points with respect to the respective LBRF. This approach is known as FFRF; see the book by Shabana [18] for a comprehensive representation. For the nodal DOF of the joint surface of the $i$th FE model, the total deformation with respect to the space fixed origin yields

$$ {}_i\mathbf{x}_{\mathrm{IJ}} = {}_i\mathbf{x}_{\mathrm{LBRF,translation}} + {}_i\mathbf{x}_{\mathrm{IJ,rotation}} + {}_i\mathbf{x}_{\mathrm{IJ,flexible}} \tag{2} $$

where the symbol ${}_i\mathbf{x}_{\mathrm{LBRF,translation}}$ represents the $(\mathbf{n}_{\mathrm{IJ}}/2 \times 1)$ vector of rigid-body translation of the joint DOF of the $i$th FE model. The $(\mathbf{n}_{\mathrm{IJ}}/2 \times 1)$ vector ${}_i\mathbf{x}_{\mathrm{IJ,rotation}}$ characterizes the rigid-body rotation of the joint DOF of the $i$th FE model. The elastic deformations of the joint DOF of the $i$th FE model relative to the rigid-body motion is represented by the $(\mathbf{n}_{\mathrm{IJ}}/2 \times 1)$ vector ${}_i\mathbf{x}_{\mathrm{IJ,flexible}}$.

Equation (2) can be written as

$$ {}_i\mathbf{x}_{\mathrm{IJ}} = \tilde{\mathbf{R}}\,{}_i\mathbf{x}_{\mathrm{LBRF}} + {}_i\tilde{\mathbf{Q}}^T\,{}^{\mathrm{LBRF}}_{i}\mathbf{x}^*_{\mathrm{IJ}} + {}_i\tilde{\mathbf{Q}}^T\,{}^{\mathrm{LBRF}}_{i}\mathbf{x}_{\mathrm{IJ,flexible}} \tag{3} $$

where $\tilde{\mathbf{R}}$ is a $(\mathbf{n}_{\mathrm{IJ}}/2 \times 3)$ transformation matrix of the form $\tilde{\mathbf{R}} = [\tilde{\mathbf{I}}_{3x3} \cdots \tilde{\mathbf{I}}_{3x3}]^T$, with the 3 by 3 identity matrix $\tilde{\mathbf{I}}_{3x3}$. The vectors ${}^{\mathrm{LBRF}}_{i}\mathbf{x}^*_{\mathrm{IJ}}$ and ${}^{\mathrm{LBRF}}_{i}\mathbf{x}_{\mathrm{IJ,flexible}}$ represent the vectors ${}_i\mathbf{x}^*_{\mathrm{IJ}}$ and ${}_i\mathbf{x}_{\mathrm{IJ,flexible}}$ expressed in the LBRF instead of the SFRF. The $(\mathbf{n}_{\mathrm{IJ}}/2 \times \mathbf{n}_{\mathrm{IJ}}/2)$ rotation matrix ${}_i\tilde{\mathbf{Q}}$ is of the form ${}_i\tilde{\mathbf{Q}} = \mathrm{diag}[{}_i\tilde{\mathbf{Q}}_{\mathrm{LBRF}}]$, where the nonzero entry ${}_i\tilde{\mathbf{Q}}_{\mathrm{LBRF}}$ represents the $(3 \times 3)$ rotation matrix of the LBRF with respect to the SFRF of the $i$th FE model.

The approximation of ${}^{\mathrm{LBRF}}_{i}\mathbf{x}_{\mathrm{IJ,flexible}}$ in Eq. (3) by a linear superposition of Ritz vectors (commonly called modes) in the form of ${}^{\mathrm{LBRF}}_{i}\mathbf{x}_{\mathrm{IJ,flexible}} \cong {}_i\tilde{\mathbf{\Phi}}_{\mathrm{IJ}}\,{}_i\mathbf{q}$ leads to

$$ {}_i\mathbf{x}_{\mathrm{IJ}} = {}_i\tilde{\mathbf{R}}\,{}_i\mathbf{x}_{\mathrm{LBRF}} + {}_i\tilde{\mathbf{Q}}^T\,{}^{\mathrm{LBRF}}_{i}\mathbf{x}^*_{\mathrm{IJ}} + {}_i\tilde{\mathbf{Q}}^T\,{}_i\tilde{\mathbf{\Phi}}_{\mathrm{IJ}}\,{}_i\mathbf{q} \tag{4} $$

The $(\mathbf{n}_{\mathrm{IJ}}/2 \times \mathbf{n}_{\mathrm{R,i}})$ matrix ${}_i\tilde{\mathbf{\Phi}}_{\mathrm{IJ}}$ contains $\mathbf{n}_{\mathrm{R,i}}$ modes to approximate the elastic joint displacements of the $i$th FE model. The corresponding modal coordinates are collected in the $(\mathbf{n}_{\mathrm{R,i}} \times 1)$ vector ${}_i\mathbf{q}$. For the application of contact laws, it may be useful to compute the relative displacement of the two joint surfaces with respect to the joint coordinate system that was introduced previously. The $(\mathbf{n}_{\mathrm{IJ}}/2 \times 1)$ vectors $\Delta^{\mathrm{IJ}}\mathbf{x}_{\mathrm{IJ}}$ and $\Delta\mathbf{x}_{\mathrm{IJ}}$ of relative displacements can be computed as

$$ \Delta^{\mathrm{IJ}}\mathbf{x}_{\mathrm{IJ}} = {}^{\mathrm{IJ}}_{1}\mathbf{x}_{\mathrm{IJ}} - {}^{\mathrm{IJ}}_{2}\mathbf{x}_{\mathrm{IJ}}, \qquad \Delta\mathbf{x}_{\mathrm{IJ}} = {}_1\mathbf{x}_{\mathrm{IJ}} - {}_1\mathbf{x}_{\mathrm{IJ}} \tag{5} $$

where the coordinates are expressed in the joint coordinate system $(\Delta^{\mathrm{IJ}}\mathbf{x}_{\mathrm{IJ}})$ or in SFRF $(\Delta\mathbf{x}_{\mathrm{IJ}})$. Considering Eq. (4) and the transformation of the relative joint displacement from the SFRF into the joint coordinate system that is attached to LBRF 1 leads to

$$ \begin{aligned} \Delta^{\mathrm{IJ}}\mathbf{x}_{\mathrm{IJ}} &= {}_1\tilde{\mathbf{Q}}_{\mathrm{IJ}}\,{}_1\tilde{\mathbf{Q}}\,\Delta\mathbf{x}_{\mathrm{IJ}} = {}_1\tilde{\mathbf{Q}}_{\mathrm{IJ}}\,{}_1\tilde{\mathbf{Q}}\{{}_1\mathbf{x}_{\mathrm{IJ}} - {}_2\mathbf{x}_{\mathrm{IJ}}\} \\ &= [\,{}_1\tilde{\mathbf{Q}}_{\mathrm{IJ}}\;{}_1\tilde{\mathbf{Q}}\;{}_1\tilde{\mathbf{R}} \quad {}_1\tilde{\mathbf{Q}}_{\mathrm{IJ}} \quad {}_1\tilde{\mathbf{Q}}_{\mathrm{IJ}}\;{}_1\tilde{\mathbf{\Phi}}_{\mathrm{IJ}}] \begin{Bmatrix} {}_1\mathbf{x}_{\mathrm{LBRF}} \\ {}^{\mathrm{LBRF}}_{1}\mathbf{x}^*_{\mathrm{IJ}} \\ {}_1\mathbf{q} \end{Bmatrix} \\ &\quad - [\,{}_1\tilde{\mathbf{Q}}_{\mathrm{IJ}}\;{}_1\tilde{\mathbf{Q}}\;{}_2\tilde{\mathbf{R}} \quad {}_1\tilde{\mathbf{Q}}_{\mathrm{IJ}}\;{}_1\tilde{\mathbf{Q}}\;{}_2\tilde{\mathbf{Q}}^T \quad {}_1\tilde{\mathbf{Q}}_{\mathrm{IJ}}\;{}_1\tilde{\mathbf{Q}}\;{}_2\tilde{\mathbf{Q}}^T\;{}_2\tilde{\mathbf{\Phi}}_{\mathrm{IJ}}] \\ &\quad \times \begin{Bmatrix} {}_2\mathbf{x}_{\mathrm{LBRF}} \\ {}^{\mathrm{LBRF}}_{2}\mathbf{x}^*_{\mathrm{IJ}} \\ {}_2\mathbf{q} \end{Bmatrix} \end{aligned} \tag{6} $$

where the $(\mathbf{n}_{\mathrm{IJ}}/2 \times \mathbf{n}_{\mathrm{IJ}}/2)$ time-invariant rotation matrix ${}_1\tilde{\mathbf{Q}}_{\mathrm{IJ}}$ transforms a vector from the LBRF coordinates of the first body into the special joint coordinate system. Note that the choice of a joint fixed coordinate system, which is attached to body 1, is arbitrary.

For common contact models, the tangential velocities between the contact surfaces are needed as well. The derivation of Eq. (6) with respect to time is straightforward from a mathematical point of view, but leads to a remarkable computational effort due to the fact that several time-dependent matrices and vectors have to be updated and multiplied with each other.

### B. Model with a Single Flexible Body

Figure 2 shows a single deformable body containing a joint interface. It is again assumed that the deformable body is modeled by using the FE method. The dots in Fig. 2 indicate the nodes of the FE model along the joint, and the other nodal DOF of the structure are omitted. The FE model has a LBRF. The area of the reference contact is known and time-invariant. The entire structure has 6 rigid-body modes in space. Consequently, all parts of the FE model have to be connected with FE modeling elements such as beams, which are indicted by a dashed line in Fig. 2. The two contact surfaces are free and congruent faces of the FE model.

A similar notation to that in the preceding section is used. Note the change in the meaning of the subscript $i$, which now denotes the attachment to the joint surface number $i$ of the same flexible body. For example, the $(\mathbf{n}_{IJ}/2 \times 1)$ vectors ${}_1\mathbf{x}_{IJ}$ and ${}_2\mathbf{x}_{IJ}$ represented the joint DOF belonging to flexible body 1 and flexible body 2, respectively, in Sec. II.A. In the present section, the corresponding symbols are denoted as $\mathbf{x}_{IJ1}$ and $\mathbf{x}_{IJ2}$. Unlike before, when each vector belonged to its own FE structure, $\mathbf{x}_{IJ1}$ and $\mathbf{x}_{IJ2}$ belong to the same FE structure. The vector $\mathbf{x}_{IJ1}$ represents the DOF of one contact surface and vector $\mathbf{x}_{IJ2}$ represents the other surface. In contrast to Sec. II.A, however, it is a problem of self-contact instead of contact.

For the sake of simplicity it is again assumed that all FE nodes of surface 1 have a unique coincident counterpart in the initial state, which belongs to surface 2:

$$\mathbf{x}^*_{IJ1} = \mathbf{x}^*_{IJ2} \tag{7}$$

As in Sec. II.A, the superscript $*$ denotes the initial state. Despite the unstressed initial state, when the joint is not sticking, Eq. (7) will not hold.

For the joint interface, the total deformation with respect to the space fixed origin yields

$$\mathbf{x}_{IJi} = \mathbf{x}_{\mathrm{LBRF,translation}} + \mathbf{x}_{IJi,\mathrm{rotation}} + \mathbf{x}_{IJi,\mathrm{flexible}} \tag{8}$$

where the symbols can be interpreted according to Eq. (2), except that the subscript $i$ now represents the contact surface $i$ instead of FE-model number $i$. The transformations from the LBRF of the flexible body into the SFRF give

$$\mathbf{x}_{IJi} = \tilde{\mathbf{R}}\mathbf{x}_{\mathrm{LBRF}} + \tilde{\mathbf{Q}}^{T\,\mathrm{LBRF}}\mathbf{x}^*_{IJi} + \tilde{\mathbf{Q}}^{T\,\mathrm{LBRF}}\mathbf{x}_{IJi,\mathrm{flexible}} \tag{9}$$

where the symbols are defined according to Eq. (3).

The elastic deformations ${}^{\mathrm{LBRF}}\mathbf{x}_{IJi,\mathrm{flexible}}$ are approximated using the modal approach in the form of ${}^{\mathrm{LBRF}}\mathbf{x}_{IJi,\mathrm{flexible}} \cong \tilde{\mathbf{\Phi}}_{IJi}\mathbf{q}$. Note that in engineering practice, $\tilde{\mathbf{\Phi}}_{IJ1}$ and $\tilde{\mathbf{\Phi}}_{IJ2}$ will be submatrices of a single mode matrix $\tilde{\mathbf{\Phi}}$ defined for the entire FE structure. In both Secs. II.A and II.B, the mode base is not continuous across the joint, such that no potential error with respect to a slope discontinuity across the interface is introduced. Adapting the considerations of Eq. (5) to the problem of a single FE model for the relative joint displacement yields

$$\Delta\mathbf{x}_{IJ} = \mathbf{x}_{IJ1} - \mathbf{x}_{IJ2} = \begin{bmatrix} \tilde{\mathbf{R}} & \tilde{\mathbf{Q}} & \tilde{\mathbf{Q}}^T\tilde{\mathbf{\Phi}}_{IJ1} \end{bmatrix} \begin{Bmatrix} \mathbf{x}_{\mathrm{LBRF}} \\ {}^{\mathrm{LBRF}}\mathbf{x}^*_{IJ1} \\ \mathbf{q} \end{Bmatrix} - \begin{bmatrix} \tilde{\mathbf{R}} & \tilde{\mathbf{Q}}^T & \tilde{\mathbf{Q}}^T\tilde{\mathbf{\Phi}}_{IJ2} \end{bmatrix} \begin{Bmatrix} \mathbf{x}_{\mathrm{LBRF}} \\ {}^{\mathrm{LBRF}}\mathbf{x}^*_{IJ2} \\ \mathbf{q} \end{Bmatrix} \tag{10}$$

The rotation matrices due to the rigid-body motion can be eliminated in Eq. (10) be using Eq. (7). Transforming the result into a joint coordinate system leads to the simple expression

$$\Delta^{IJ}\mathbf{x}_{IJ} = \tilde{\mathbf{Q}}_{IJ}\tilde{\mathbf{Q}}\Delta\mathbf{x}_{IJ} = \tilde{\mathbf{Q}}_{IJ}(\tilde{\mathbf{\Phi}}_{IJ1} - \tilde{\mathbf{\Phi}}_{IJ2})\mathbf{q} = {}^{IJ}\tilde{\mathbf{\Phi}}_{\Delta IJ}\mathbf{q} \tag{11}$$

where ${}^{IJ}\tilde{\mathbf{\Phi}}_{\Delta IJ}$ is the $(\mathbf{n}_{IJ}/2 \times \mathbf{n}_R)$ matrix of modes of relative displacement of joint surfaces 1 and 2 with respect to the joint coordinate system. The rotation matrix $\tilde{\mathbf{Q}}_{IJ}$ transforms a vector from LBRF into the joint coordinate system. Note that ${}^{IJ}\tilde{\mathbf{\Phi}}_{\Delta IJ}$ is time-invariant and needs to be computed just once, at the beginning of a simulation.

The relative velocities can be easily computed by

$$\Delta^{IJ}\dot{\mathbf{x}}_{IJ} = {}^{IJ}\tilde{\mathbf{\Phi}}_{\Delta IJ}\dot{\mathbf{q}} \tag{12}$$

where the dot denotes the first derivative with respect to the time.

### C. Summary

Comparing Eqs. (6) and (11) leads to the conclusion that a flexible structure represented in FFRF, which consists of two jointed substructures, in principle, should be modeled as one single flexible body. This leads to a significant savings of computational effort and will be applied subsequently.

The next section deals with the question of how the mode base of the single body can be properly selected to prescribe the relative displacements occurring in the joint interface.

## III. Joint Interface Modes

### A. Problem Formulation

Figure 3 shows a flexible body modeled by the FE method that contains a joint interface. A finite element model with $n$ nodal degrees of freedom is considered. The total structure consists of two jointed substructures. The vector $\mathbf{x}$ represents the $n$ DOF of the whole structure. External forces, which are represented by the $(\mathbf{n} \times 1)$ vector $\mathbf{f}$, are acting on the structure exclusively via the nodes $B$.

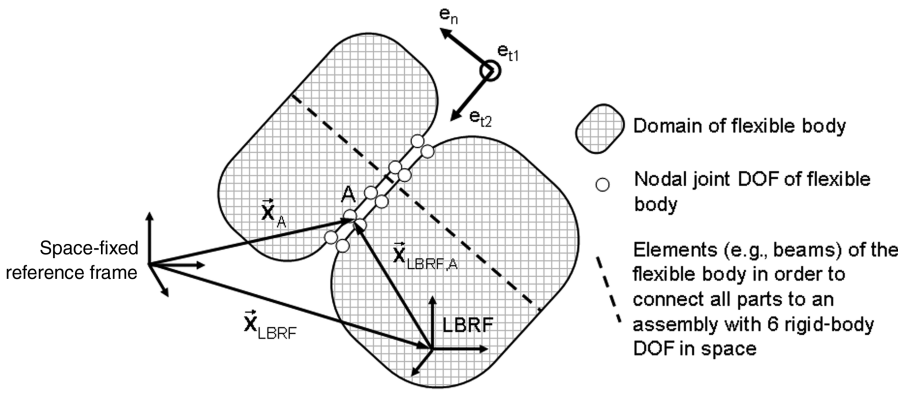


**Fig. 2 One deformable body with an integrated interface (joint).**

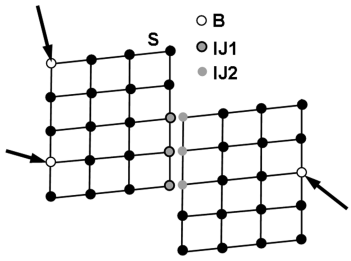


**Fig. 3 FE model with a joint.**

The nodal DOF of $B$ are collected in the vector $\mathbf{x}_B$, which is of the dimension $(\mathbf{n}_B \times 1)$, and are indicated in Fig. 3 by white dots. The nonlinear contact forces, which are represented by the $(\mathbf{n} \times 1)$ vector $\mathbf{f}_{\text{joint}}$, act on the nodal DOF of the joint, which are collected in the $(\mathbf{n}_{IJ} \times 1)$ vector $\mathbf{x}_{IJ}$, and are indicated in Fig. 3 by gray dots. Note that IJ represents an internal joint interface and not a support. The joint interface in which the contact forces will act during the mode-based simulation consists at the stage of the generation of the mode base of two congruent surfaces. It is moreover assumed that the joint undergoes just small deformations and small relative displacements. In practice, this is a restriction that is suitable for a large class of joints, such as bolted joints, riveted joints, glued joints, spot-welded seams, and many more.

According to Fig. 3, it is possible to subdivide IJ into the DOF of the involved faces IJ1 and IJ2. For simplicity, it is assumed that IJ1 and IJ2 do have coincident nodes at the initial state. This is not a limitation to the generality of the proposed algorithm. According to the preceding scheme, the vector $\mathbf{x}_{IJ}$ can be subdivided into $\mathbf{x}_{IJ1}$ and $\mathbf{x}_{IJ2}$, which are both of the dimension $(\mathbf{n}_{IJ}/2 \times 1)$. The remaining inner DOF are represented by the $(\mathbf{n}_{I\setminus IJ} \times 1)$ vector $\mathbf{x}_{I\setminus IJ}$ and are indicated by the black dots in Fig. 3. According to the preceding scheme, the vector of DOF can be written as

$$\mathbf{x} = \begin{Bmatrix} \mathbf{x}_B \\ \mathbf{x}_{IJ} \\ \mathbf{x}_{I\setminus IJ} \end{Bmatrix} = \begin{Bmatrix} \mathbf{x}_B \\ \mathbf{x}_{IJ1} \\ \mathbf{x}_{IJ2} \\ \mathbf{x}_{I\setminus IJ} \end{Bmatrix} \tag{13}$$

and the vectors of forces take the form

$$\mathbf{f} = \begin{Bmatrix} \mathbf{f}_B \\ \mathbf{0} \\ \mathbf{0} \end{Bmatrix} \quad \text{and} \quad \mathbf{f}_{\text{joint}} = \begin{Bmatrix} \mathbf{0} \\ \mathbf{f}_{IJ} \\ \mathbf{0} \end{Bmatrix} \tag{14}$$

In the following, we restrict ourselves to the case of no rigid-body motions being superimposed upon the single flexible body. The reason is that a consideration of small deformations in the aforementioned FFRF for multibody dynamic systems nowadays is standard and can be performed by commercial codes. What is necessary is to have a suitable and efficient mode basis at hand; again, see the book by Shabana [18] for questions concerning multibody dynamic systems. It is therefore sufficient to study the efficiency of a mode basis using vibrations about equilibrium positions only.

The equation of motion can then be expressed as

$$\begin{bmatrix} \tilde{\mathbf{M}}_{B,B} & \tilde{\mathbf{M}}_{B,IJ} & \tilde{\mathbf{M}}_{B,I\setminus IJ} \\ & \tilde{\mathbf{M}}_{IJ,IJ} & \tilde{\mathbf{M}}_{IJ,I\setminus IJ} \\ \text{sym} & & \tilde{\mathbf{M}}_{I\setminus IJ,I\setminus IJ} \end{bmatrix} \begin{Bmatrix} \ddot{\mathbf{x}}_B \\ \ddot{\mathbf{x}}_{IJ} \\ \ddot{\mathbf{x}}_{I\setminus IJ} \end{Bmatrix} + \begin{bmatrix} \tilde{\mathbf{K}}_{B,B} & \tilde{\mathbf{K}}_{B,IJ} & \tilde{\mathbf{K}}_{B,I\setminus IJ} \\ & \tilde{\mathbf{K}}_{IJ,IJ} & \tilde{\mathbf{K}}_{IJ,I\setminus IJ} \\ \text{sym} & & \tilde{\mathbf{K}}_{I\setminus IJ,I\setminus IJ} \end{bmatrix} \begin{Bmatrix} \mathbf{x}_B \\ \mathbf{x}_{IJ} \\ \mathbf{x}_{I\setminus IJ} \end{Bmatrix} = \mathbf{f} + \mathbf{f}_{\text{joint}} \tag{15}$$

where the $(\mathbf{n} \times \mathbf{n})$ symmetric mass matrix $\tilde{\mathbf{M}}$ and the $(\mathbf{n} \times \mathbf{n})$ symmetric stiffness matrix $\tilde{\mathbf{K}}$ are subdivided according to the definition of DOF previously given.

### B. Modal Reduction

Modal reduction methods have in common that a set of vectors (commonly called modes) are used to approximate the physical displacements of the structure in the form of

$$\mathbf{x} \cong \tilde{\mathbf{\Phi}}\mathbf{q} \tag{16}$$

The time-invariant $(\mathbf{n} \times \mathbf{n}_R)$ modal transformation matrix $\tilde{\mathbf{\Phi}}$ considers $\mathbf{n}_R$ modes and can be written as $\tilde{\mathbf{\Phi}} = [\boldsymbol{\varphi}_1\ \boldsymbol{\varphi}_2\ \boldsymbol{\varphi}_3\ \cdots\ \boldsymbol{\varphi}_{\mathbf{n}_R}]$. The $(\mathbf{n}_R \times 1)$ vector $\mathbf{q}$ represents the generalized coordinates. Substituting Eq. (16) into Eq. (15), together with the principle of virtual work (which requires that for an arbitrary virtual displacement $\delta\mathbf{x} \cong \tilde{\mathbf{\Phi}}\delta\mathbf{q}$, the virtual work $\delta\mathbf{x}^T\{\tilde{\mathbf{M}}\ddot{\mathbf{x}} + \tilde{\mathbf{K}}\mathbf{x} - \mathbf{f} - \mathbf{f}_{\text{joint}}\}$ vanishes) gives

$$\tilde{\mathbf{M}}_{\text{trans}}\ddot{\mathbf{q}} + \tilde{\mathbf{K}}_{\text{trans}}\mathbf{q} = \mathbf{f}_{\text{trans}} + \mathbf{f}_{\text{joint–trans}} \tag{17}$$

where

$$\tilde{\mathbf{M}}_{\text{trans}} = \tilde{\mathbf{\Phi}}^T\tilde{\mathbf{M}}\tilde{\mathbf{\Phi}} \quad \tilde{\mathbf{K}}_{\text{trans}} = \tilde{\mathbf{\Phi}}^T\tilde{\mathbf{K}}\tilde{\mathbf{\Phi}} \quad \mathbf{f}_{\text{trans}} = \tilde{\mathbf{\Phi}}^T\mathbf{f} \quad \mathbf{f}_{\text{joint–trans}} = \tilde{\mathbf{\Phi}}^T\mathbf{f}_{\text{joint}}$$

The dimension of the transformed system (17) is $\mathbf{n}_R$. The reduction of the system is obtained by using a suitable set of modes having a dimension $\mathbf{n}_R$ of the transformed system (17), which is much smaller than the dimension $n$ of the original system (15) ($\mathbf{n}_R \ll \mathbf{n}$), but producing a sufficiently low error.

The modal reduction methods known from the literature lead to a satisfying balance between accuracy and computational effort of the system (15) if $\mathbf{f}_{\text{joint}}$ is zero and the value of $\mathbf{n}_B$ is not too large, because each DOF of $\mathbf{x}_B$ leads to a corresponding mode (and therefore DOF) in the transformed system (17). As an example, the Craig–Bampton mode base is mentioned, in which each entry in $\mathbf{x}_B$ leads to a so-called constraint mode [10]. If the contact force $\mathbf{f}_{\text{joint}}$ is treated in the same way as $\mathbf{f}$, the classical reduction methods will lose their efficiency because, in general, $\mathbf{f}_{\text{joint}}$ is a distributed force and the number of DOF $\mathbf{n}_{IJ}$ is therefore large.

The key goal of the present work is an extension of existing mode bases to overcome the mentioned efficiency problem. This JIMS extension takes an important mechanical property of joints explicitly into account: namely, that Newton's third law should be satisfied across the interface. Consequently, the proposed modal transformation is written as

$$\mathbf{x} \cong \tilde{\mathbf{\Phi}}\mathbf{q} = \left[\, \tilde{\mathbf{\Phi}}^{\text{classical}} \quad \tilde{\mathbf{\Phi}}^{\text{JIM}} \,\right]\mathbf{q} \tag{18}$$

where the $(\mathbf{n} \times \mathbf{n}_C)$ matrix $\tilde{\mathbf{\Phi}}^{\text{classical}}$ represents any known mode base that is suitable for system (15) if $\mathbf{f}_{\text{joint}}$ is zero. Usually, $\tilde{\mathbf{\Phi}}^{\text{classical}}$ results from a preliminary FE computation, assuming that there is no interface to present. The $(\mathbf{n} \times \mathbf{n}_{\text{JIM}})$ matrix $\tilde{\mathbf{\Phi}}_{\text{JIM}}$ gathers the proposed JIMs. The total number of regarded modes $\mathbf{n}_R$ is $\mathbf{n}_R = \mathbf{n}_C + \mathbf{n}_{\text{JIM}}$. Before the computation of JIMs is discussed in Secs. III.D and III.E, the following fundamental property of joints is reviewed.

### C. Equivalence of Forces Acting upon the Two Surfaces of a Joint

Figure 4 outlines a joint connecting surfaces 1 and 2; the forces $\mathbf{t}_{IJ1(\mathbf{x}_{A1})}$ and $\mathbf{t}_{IJ2(\mathbf{x}_{A2})}$ act on these two surfaces. For a common interface point in space, $\mathbf{x}_{A1} = \mathbf{x}_{A2} = \mathbf{x}_A^0$, the principle of action equal to reaction requires $\mathbf{t}_{IJ1(\mathbf{x}_A^0)} = -\mathbf{t}_{IJ2(\mathbf{x}_A^0)}$ (see, for example, Laursen [20]). This will be also be subsequently denoted as the principle of equivalence. Because the principle action equal to reaction dates back to Sir Isaac Newton, we also talk about Newton's third law.

In the framework of an FE model, the latter principle of equivalence requires that the vector of joint forces in the equation of motion (15) has to be of the form

$$\mathbf{f}_{\text{joint}}^T = \left[\, \mathbf{0}^T \quad \mathbf{f}_{IJ1}^T \quad -\mathbf{f}_{IJ1}^T \quad 0^T \,\right] \tag{19}$$

Note that the scope of application of the proposed JIMs is to assure, at least to a certain extent, the validity of Eq. (19). This is because the

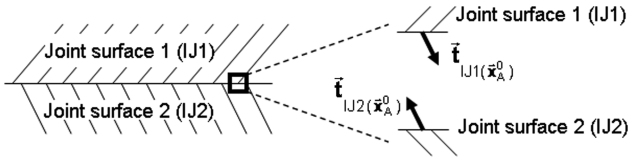


**Fig. 4 Local equivalence of forces along the joint surfaces.**

particular form of $\mathbf{f}_{\text{joint}}$ will subsequently be explicitly taken into account at the stage of JIM generation.

### D. Direct Computation of JIMs

Applying the latter principle of equivalence to the equation of motion (15), subdividing $\mathbf{x}_{\text{IJ}}$ into $\mathbf{x}_{\text{IJ1}}$ and $\mathbf{x}_{\text{IJ2}}$, and neglecting the inertia terms leads to

$$\begin{bmatrix} \tilde{\mathbf{K}}_{B,B} & \tilde{\mathbf{K}}_{B,\text{IJ1}} & \tilde{\mathbf{K}}_{B,\text{IJ2}} & \tilde{\mathbf{K}}_{B,I\setminus\text{IJ}} \\ & \tilde{\mathbf{K}}_{\text{IJ1,IJ1}} & \tilde{\mathbf{K}}_{\text{IJ1,IJ2}} & \tilde{\mathbf{K}}_{\text{IJ1},I\setminus\text{IJ}} \\ & & \tilde{\mathbf{K}}_{\text{IJ2,IJ2}} & \tilde{\mathbf{K}}_{\text{IJ2},I\setminus\text{IJ}} \\ \text{sym} & & & \tilde{\mathbf{K}}_{I\setminus\text{IJ},I\setminus\text{IJ}} \end{bmatrix} \begin{Bmatrix} \mathbf{x}_B \\ \mathbf{x}_{\text{IJ1}} \\ \mathbf{x}_{\text{IJ2}} \\ \mathbf{x}_{I\setminus\text{IJ}} \end{Bmatrix} = \begin{Bmatrix} \mathbf{f}_B \\ \mathbf{0} \\ \mathbf{0} \\ \mathbf{0} \end{Bmatrix} + \begin{Bmatrix} \mathbf{0} \\ \mathbf{f}_{\text{IJ1}} \\ -\mathbf{f}_{\text{IJ1}} \\ \mathbf{0} \end{Bmatrix} \tag{20}$$

Note that the desired JIMs are defined as an extension to a mode base that is already suitable to approximate all possible motions of $\mathbf{x}_B$. Consequently, the DOF of $\mathbf{x}_B$ need not to be considered any more and will be constrained to zero in the further considerations, for the sake of brevity. The last row of Eq. (20) now enables expressing $\mathbf{x}_{I\setminus\text{IJ}}$ as a function of $\mathbf{x}_{\text{IJ1}}$ and $\mathbf{x}_{\text{IJ2}}$:

$$\mathbf{x}_{I\setminus\text{IJ}} = -[\tilde{\mathbf{K}}_{I\setminus\text{IJ},I\setminus\text{IJ}}]^{-1} + \{\tilde{\mathbf{K}}_{I\setminus\text{IJ},\text{IJ1}}\mathbf{x}_{\text{IJ1}} + \tilde{\mathbf{K}}_{I\setminus\text{IJ},\text{IJ2}}\mathbf{x}_{\text{IJ2}}\} \tag{21}$$

Setting the second row of Eq. (20) to be equivalent to the negative of the third row (principle of equivalence) and substituting $\mathbf{x}_{I\setminus\text{IJ}}$ by Eq. (21) leads to

$$\begin{aligned} \mathbf{x}_{\text{IJ1}} = {} & [\tilde{\mathbf{K}}_{\text{IJ1,IJ1}} + \tilde{\mathbf{K}}_{\text{IJ2,IJ1}} - [\tilde{\mathbf{K}}_{\text{IJ1},I\setminus\text{IJ}} + \tilde{\mathbf{K}}_{\text{IJ2},I\setminus\text{IJ}}] \\ & \times [\tilde{\mathbf{K}}_{I\setminus\text{IJ},I\setminus\text{IJ}}]^{-1}\tilde{\mathbf{K}}_{I\setminus\text{IJ},\text{IJ1}}]^{-1}[[\tilde{\mathbf{K}}_{\text{IJ1},I\setminus\text{IJ}} + \tilde{\mathbf{K}}_{\text{IJ2},I\setminus\text{IJ}}] \\ & \times [\tilde{\mathbf{K}}_{I\setminus\text{IJ},I\setminus\text{IJ}}]^{-1}\tilde{\mathbf{K}}_{I\setminus\text{IJ},\text{IJ2}} - \tilde{\mathbf{K}}_{\text{IJ1,IJ2}} - \tilde{\mathbf{K}}_{\text{IJ2,IJ2}}]\mathbf{x}_{\text{IJ2}} = {}_{\#}\tilde{\mathbf{G}}\mathbf{x}_{\text{IJ2}} \end{aligned} \tag{22}$$

For the sake of clarity, all matrices of this section are marked with a hash sign to distinguish them from those of Sec. III.E. Note that the $(\mathbf{n}_{\text{IJ}}/2 \times \mathbf{n}_{\text{IJ}}/2)$ matrix ${}_{\#}\tilde{\mathbf{G}}$ gives the effect of $\mathbf{x}_{\text{IJ2}}$ upon $\mathbf{x}_{\text{IJ1}}$, taking into account the principle of equivalence in a quasi-static approximation. Setting

$$\begin{Bmatrix} \mathbf{x}_B \\ \mathbf{x}_{\text{IJ1}} \\ \mathbf{x}_{\text{IJ2}} \\ \mathbf{x}_{I\setminus\text{IJ}} \end{Bmatrix} = \begin{bmatrix} \tilde{\mathbf{0}} \\ {}_{\#}\tilde{\mathbf{G}} \\ \tilde{\mathbf{I}} \\ -[\tilde{\mathbf{K}}_{I\setminus\text{IJ},I\setminus\text{IJ}}]^{-1}[\tilde{\mathbf{K}}_{I\setminus\text{IJ},\text{IJ1}\#}\tilde{\mathbf{G}} + \tilde{\mathbf{K}}_{I\setminus\text{IJ},\text{IJ2}}] \end{bmatrix} \mathbf{x}_{\text{IJ2}} = {}_{\#}\tilde{\mathbf{H}}\mathbf{x}_{\text{IJ2}} \tag{23}$$

the equation of motion (15) can be reduced into a system of dimension $\mathbf{n}_{\text{IJ}}/2$ as

$${}_{\#}\tilde{\mathbf{M}}_{\text{red,IJ2}}\ddot{\mathbf{x}}_{\text{IJ2}} + {}_{\#}\tilde{\mathbf{K}}_{\text{red,IJ2}}\mathbf{x}_{\text{IJ2}} = {}_{\#}\mathbf{f}_{\text{red,IJ2}} \tag{24}$$

where

$${}_{\#}\tilde{\mathbf{M}}_{\text{red,IJ2}} = {}_{\#}\tilde{\mathbf{H}}^T\tilde{\mathbf{M}}_{\#}\tilde{\mathbf{H}} \qquad {}_{\#}\tilde{\mathbf{K}}_{\text{red,IJ2}} = {}_{\#}\tilde{\mathbf{H}}^T\tilde{\mathbf{K}}_{\#}\tilde{\mathbf{H}}$$

$${}_{\#}\mathbf{f}_{\text{red,IJ2}} = {}_{\#}\tilde{\mathbf{H}}^T\begin{bmatrix} \mathbf{f}_B^T & \mathbf{f}_{\text{IJ1}}^T & -\mathbf{f}_{\text{IJ1}}^T & \mathbf{0}^T \end{bmatrix}^T$$

The eigenvalue problem of the reduced equation of motion (24) gives the JIMs for $\mathbf{x}_{\text{IJ2}}$ and can be written as

$$({}_{\#}\tilde{\mathbf{K}}_{\text{red,IJ2}} - ({}_{\#}\tilde{\boldsymbol{\Omega}}^{\text{JIM}})^2{}_{\#}\tilde{\mathbf{M}}_{\text{red,IJ2}})^*_{\#}\tilde{\boldsymbol{\Phi}}^{\text{JIM}}_{\text{IJ2}} = \tilde{\mathbf{0}} \tag{25}$$

where ${}_{\#}\tilde{\boldsymbol{\Omega}}^{\text{JIM}}$ is the $(\mathbf{n}_{\text{IJ}}/2 \times \mathbf{n}_{\text{IJ}}/2)$ diagonal matrix of eigenvalues, and ${}^*_{\#}\tilde{\boldsymbol{\Phi}}^{\text{JIM}}_{\text{IJ2}}$ is the $(\mathbf{n}_{\text{IJ}}/2 \times \mathbf{n}_{\text{IJ}}/2)$ matrix of joint interface modes for the joint surface IJ2. Note that Eq. (25) has $\mathbf{n}_{\text{IJ}}/2$ solutions, but it is to be expected that a truncated set of eigenvectors ${}_{\#}\tilde{\boldsymbol{\Phi}}^{\text{JIM}}_{\text{IJ2}}$ of the dimension $(\mathbf{n}_{\text{IJ}}/2 \times \mathbf{n}_{\text{JIM}})$ will deliver excellent results ($\mathbf{n}_{\text{JIM}} \ll \mathbf{n}_{\text{IJ}}/2$).

Finally, the JIMs need to be statically extended from the joint surface $\mathbf{x}_{\text{IJ2}}$ to the entire structure. This leads to

$$\begin{aligned} {}_{\#}\tilde{\boldsymbol{\Phi}}^{\text{JIM}} &= \begin{bmatrix} {}_{\#}\tilde{\boldsymbol{\Phi}}^{\text{JIM}}_{B} \\ {}_{\#}\tilde{\boldsymbol{\Phi}}^{\text{JIM}}_{\text{IJ1}} \\ {}_{\#}\tilde{\boldsymbol{\Phi}}^{\text{JIM}}_{\text{IJ2}} \\ {}_{\#}\tilde{\boldsymbol{\Phi}}^{\text{JIM}}_{\text{I\setminus IJ}} \end{bmatrix} = {}_{\#}\tilde{\mathbf{H}}_{\#}\tilde{\boldsymbol{\Phi}}^{\text{JIM}}_{\text{IJ2}} \\ &= \begin{bmatrix} \tilde{\mathbf{0}} \\ {}_{\#}\tilde{\mathbf{G}}_{\#}\tilde{\boldsymbol{\Phi}}^{\text{JIM}}_{\text{IJ2}} \\ {}_{\#}\tilde{\boldsymbol{\Phi}}^{\text{JIM}}_{\text{IJ2}} \\ -\left[\tilde{\mathbf{K}}_{I\setminus\text{IJ},I\setminus\text{IJ}}\right]^{-1}\left[\tilde{\mathbf{K}}_{I\setminus\text{IJ},\text{IJ1}\#}\tilde{\mathbf{G}} + \tilde{\mathbf{K}}_{I\setminus\text{IJ},\text{IJ2}}\right]_{\#}\tilde{\boldsymbol{\Phi}}^{\text{JIM}}_{\text{IJ2}} \end{bmatrix} \end{aligned} \tag{26}$$

which is the matrix of JIMs introduced in Eq. (18). Note that the column number $i$ of the $(\mathbf{n} \times \mathbf{n}_{\text{JIM}})$ matrix ${}_{\#}\tilde{\boldsymbol{\Phi}}^{\text{JIM}}$ represents the exact static response of the entire structure, due to the imposed deformations $\mathbf{x}_B = \mathbf{0}$, $\mathbf{x}_{\text{IJ1}} = {}_{\#}\tilde{\mathbf{G}}\{{}_{\#}\tilde{\boldsymbol{\varphi}}^{\text{JIM}}_{\text{IJ2}}\}_i$ and $\mathbf{x}_{\text{IJ2}} = \{{}_{\#}\tilde{\boldsymbol{\varphi}}^{\text{JIM}}_{\text{IJ2}}\}_i$, where $\{{}_{\#}\tilde{\boldsymbol{\varphi}}^{\text{JIM}}_{\text{IJ2}}\}_i$ is the column number $i$ of ${}_{\#}\tilde{\boldsymbol{\Phi}}^{\text{JIM}}_{\text{IJ2}}$. Note furthermore that the quasi-static relation (20) has been used only to approximate $\mathbf{x}_{\text{IJ1}}$ by $\mathbf{x}_{\text{IJ2}}$, but that the full inertia matrix $\tilde{\mathbf{M}}$ has been considered from Eq. (24) and onward.

### E. Computation of JIMs Based on Statically Reduced Matrices

An alternative method for the computation of JIMs starts with the static reduction of the mass and stiffness matrices of system (15) to $\mathbf{x}_{\text{IJ}}$. Following the method of Guyan [8], the reduced stiffness matrix $\tilde{\mathbf{K}}^{\text{red}}_{\text{IJ}}$ takes the form

$$\tilde{\mathbf{K}}^{\text{red}}_{\text{IJ}} = (\tilde{\mathbf{K}}_{\text{IJ,IJ}} - \tilde{\mathbf{K}}_{\text{IJ},I\setminus\text{IJ}}\tilde{\mathbf{K}}^{-1}_{I\setminus\text{IJ},I\setminus\text{IJ}}\tilde{\mathbf{K}}_{I\setminus\text{IJ,IJ}}) \tag{27}$$

and the reduced mass matrix $\tilde{\mathbf{M}}^{\text{red}}_{\text{IJ}}$ can be written as

$$\begin{aligned} \tilde{\mathbf{M}}^{\text{red}}_{\text{IJ}} = {} & \tilde{\mathbf{M}}_{\text{IJ,IJ}} - \tilde{\mathbf{M}}_{\text{IJ},I\setminus\text{IJ}}\tilde{\mathbf{K}}^{-1}_{I\setminus\text{IJ},I\setminus\text{IJ}}\tilde{\mathbf{K}}_{I\setminus\text{IJ,IJ}} \\ & - (\tilde{\mathbf{K}}^{-1}_{I\setminus\text{IJ},I\setminus\text{IJ}}\tilde{\mathbf{K}}_{I\setminus\text{IJ,IJ}})^T(\tilde{\mathbf{M}}_{I\setminus\text{IJ,IJ}} - \tilde{\mathbf{M}}_{I\setminus\text{IJ},I\setminus\text{IJ}}\tilde{\mathbf{K}}^{-1}_{I\setminus\text{IJ},I\setminus\text{IJ}}\tilde{\mathbf{K}}_{I\setminus\text{IJ,IJ}}) \end{aligned} \tag{28}$$

For the Guyan reduction, the DOF of $\mathbf{x}_B$ are set to $\mathbf{0}$, and it is assumed that restraining $\mathbf{x}_B$ does not permit any rigid-body motion of the structure. Refer to Eq. (20) for a more detailed explanation of the latter assumption. Solving an eigenvalue problem using the matrices $\tilde{\mathbf{K}}^{\text{red}}_{\text{IJ}}$ and $\tilde{\mathbf{M}}^{\text{red}}_{\text{IJ}}$ leads to modes that are referred to in the literature as interface modes (IMs) (see Tran [13]). IMs represent a suitable approximation of the deformation in a joint as well. A comparison of the proposed JIMs with the IMs is performed in Sec. IV.A. For the sake of comparison, the computation of the IMs is briefly reviewed in Sec. III.H. Recall here that for the generation of the IMs the principle of equivalence is not taken into account.

Applying the principle of equivalence (refer to Sec. III.C) to the statically reduced system leads to

$$\begin{bmatrix} [\tilde{\mathbf{M}}_{\text{red,IJ}}]_{11} & [\tilde{\mathbf{M}}_{\text{red,IJ}}]_{12} \\ \text{sym} & [\tilde{\mathbf{M}}_{\text{red,IJ}}]_{22} \end{bmatrix} \begin{Bmatrix} \ddot{\mathbf{x}}_{\text{IJ1}} \\ \ddot{\mathbf{x}}_{\text{IJ2}} \end{Bmatrix} + \begin{bmatrix} [\tilde{\mathbf{K}}_{\text{red,IJ}}]_{11} & [\tilde{\mathbf{K}}_{\text{red,IJ}}]_{12} \\ \text{sym} & [\tilde{\mathbf{K}}_{\text{red,IJ}}]_{22} \end{bmatrix} \begin{Bmatrix} \mathbf{x}_{\text{IJ1}} \\ \mathbf{x}_{\text{IJ2}} \end{Bmatrix} = \begin{Bmatrix} \mathbf{f}_{\text{IJ1}} \\ -\mathbf{f}_{\text{IJ1}} \end{Bmatrix} \tag{29}$$

where the matrices $\tilde{\mathbf{K}}^{\text{red}}_{\text{IJ}}$ and $\tilde{\mathbf{M}}^{\text{red}}_{\text{IJ}}$ are subdivided accordingly. If the inertia forces are omitted, Eq. (29) yields an approximation to express $\mathbf{x}_{\text{IJ1}}$ as a function of $\mathbf{x}_{\text{IJ2}}$:

$$\mathbf{x}_{IJ1} = -[[\tilde{\mathbf{K}}_{red,IJ}]_{11} + [\tilde{\mathbf{K}}_{red,IJ}]_{21}]^{-1}[[\tilde{\mathbf{K}}_{red,IJ}]_{22} + [\tilde{\mathbf{K}}_{red,IJ}]_{12}]\mathbf{x}_{IJ2} = \tilde{\mathbf{G}}\mathbf{x}_{IJ2} \tag{30}$$

As in the preceding section, a $(\mathbf{n}_{IJ}/2 \times \mathbf{n}_{IJ}/2)$ matrix $\tilde{\mathbf{G}}$ is obtained that gives the effect of $\mathbf{x}_{IJ2}$ upon $\mathbf{x}_{IJ1}$, taking into account the principle of equivalence in the joint. With the transformation rule

$$\begin{Bmatrix} \mathbf{x}_{IJ1} \\ \mathbf{x}_{IJ2} \end{Bmatrix} = \begin{bmatrix} \tilde{\mathbf{G}} \\ \tilde{\mathbf{I}} \end{bmatrix} \mathbf{x}_{IJ2} = \tilde{\mathbf{H}}\mathbf{x}_{IJ2} \tag{31}$$

the already reduced equation of motion (29) can be reduced again and takes the form

$$\tilde{\mathbf{M}}_{red,IJ2}\ddot{\mathbf{x}}_{IJ2} + \tilde{\mathbf{K}}_{red,IJ2}\mathbf{x}_{IJ2} = \mathbf{f}_{red,IJ2} \tag{32}$$

where

$$\tilde{\mathbf{M}}_{red,IJ2} = \tilde{\mathbf{H}}^T\tilde{\mathbf{M}}_{red,IJ}\tilde{\mathbf{H}}$$
$$\tilde{\mathbf{K}}_{red,IJ2} = \tilde{\mathbf{H}}^T\tilde{\mathbf{K}}_{red,IJ2}\tilde{\mathbf{H}}$$
$$\mathbf{f}_{red,IJ2} = \tilde{\mathbf{H}}^T\begin{Bmatrix} \mathbf{f}_{IJ1} \\ -\mathbf{f}_{IJ1} \end{Bmatrix}$$

The JIMs are obtained from the solution of the eigenproblem with the doubly reduced $(\mathbf{n}_{IJ}/2 \times \mathbf{n}_{IJ}/2)$ matrices $\tilde{\mathbf{M}}_{red,IJ2}$ and $\tilde{\mathbf{K}}_{red,IJ2}$, which can be written as

$$(\tilde{\mathbf{K}}_{red,IJ2} - (\tilde{\mathbf{\Omega}}^{JIM})^2\tilde{\mathbf{M}}_{red,IJ2})^*\tilde{\mathbf{\Phi}}^{JIM}_{IJ2} = \tilde{\mathbf{0}} \tag{33}$$

where $\tilde{\mathbf{\Omega}}^{JIM}$ is the $(\mathbf{n}_{IJ}/2 \times \mathbf{n}_{IJ}/2)$ diagonal matrix of eigenvalues and ${}^*\tilde{\mathbf{\Phi}}^{JIM}_{IJ2}$ is the $(\mathbf{n}_{IJ}/2 \times \mathbf{n}_{IJ}/2)$ matrix of JIMs for the joint surface IJ2. Equation (33) has $\mathbf{n}_{IJ}/2$ solutions, but it is to be expected that a truncated set of eigenvectors $\tilde{\mathbf{\Phi}}^{JIM}_{IJ2}$ of the dimension $(\mathbf{n}_{IJ}/2 \times \mathbf{n}_{JIM})$ will deliver satisfying results $(\mathbf{n}_{JIM} \ll \mathbf{n}_{IJ}/2)$. As in the section before, it is necessary to extend the JIMs of $\mathbf{x}_{IJ2}$ to the entire structure. The $(\mathbf{n} \times \mathbf{n}_{JIM})$ matrix $\tilde{\mathbf{\Phi}}^{JIM}$ of JIMs considering all DOF of the system takes the form

$$\tilde{\mathbf{\Phi}}^{JIM} = \begin{bmatrix} \tilde{\mathbf{\Phi}}^{JIM}_{B} \\ \tilde{\mathbf{\Phi}}^{JIM}_{IJ1} \\ \tilde{\mathbf{\Phi}}^{JIM}_{IJ2} \\ \tilde{\mathbf{\Phi}}^{JIM}_{I\setminus IJ} \end{bmatrix} = \begin{bmatrix} \tilde{\mathbf{0}} \\ \tilde{\mathbf{G}}\tilde{\mathbf{\Phi}}^{JIM}_{IJ2} \\ \tilde{\mathbf{\Phi}}^{JIM}_{IJ2} \\ -\tilde{\mathbf{K}}^{-1}_{I\setminus IJ,I\setminus IJ}\tilde{\mathbf{K}}_{I\setminus IJ,IJ}\begin{bmatrix} \tilde{\mathbf{G}}\tilde{\mathbf{\Phi}}^{JIM}_{IJ2} \\ \tilde{\mathbf{\Phi}}^{JIM}_{IJ2} \end{bmatrix} \end{bmatrix} \tag{34}$$

As in the preceding section, the column number $i$ of $\tilde{\mathbf{\Phi}}^{JIM}$ represents the exact static response of the entire structur, e due to the imposed deformations $\mathbf{x}_B = \mathbf{0}$, $\mathbf{x}_{IJ1} = \tilde{\mathbf{G}}\{\varphi^{JIM}_{IJ2}\}_i$ and $\mathbf{x}_{IJ2} = \tilde{\mathbf{G}}\{\varphi^{JIM}_{IJ2}\}_i$. The vector $\{\varphi^{JIM}_{IJ2}\}_i$ is the JIM corresponding to the column number $i$ of the matrix $\tilde{\mathbf{\Phi}}^{JIM}_{IJ2}$.

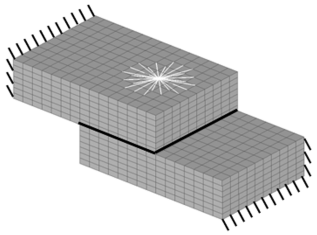

**Fig. 5 Simple jointed beam structure with solid and wire-frame representation.**

### F. Investigation of the Correlation of the JIMs Computed by the Preceding Methods

The modal assurance criterion (MAC) is a widely used method to compare two sets of modes. For details concerning the MAC, refer to Allemang and Brown [21]. Using the MAC for a comparison of the directly computed JIMs of Eq. (26) with the JIMs computed via reduced mass and stiffness matrices according to Eq. (34) leads to

$$\mathrm{MAC}\left(\left\{{}_{\#}\varphi^{JIM}_{IJ}\right\}_i, \left\{\varphi^{JIM}_{IJ}\right\}_j\right) = \frac{\left(\left\{{}_{\#}\varphi^{JIM}_{IJ}\right\}_i^T\left\{\varphi^{JIM}_{IJ}\right\}_j\right)^2}{\left(\left\{{}_{\#}\varphi^{JIM}_{IJ}\right\}_i^T\left\{{}_{\#}\varphi^{JIM}_{IJ}\right\}_i\right)\left(\left\{\varphi^{JIM}_{IJ}\right\}_j^T\left\{\varphi^{JIM}_{IJ}\right\}_j\right)} \tag{35}$$

where $\mathrm{MAC}(\{{}_{\#}\varphi^{JIM}_{IJ}\}_i, \{\varphi^{JIM}_{IJ}\}_j)$ is the scalar MAC value for the $(\mathbf{n}_{IJ} \times 1)$ vector $\{{}_{\#}\varphi^{JIM}_{IJ}\}_i$ corresponding to the column number $i$ of ${}_{\#}\tilde{\mathbf{\Phi}}^{JIM}_{IJ}$ and the $(\mathbf{n}_{IJ} \times 1)$ vector $\{\varphi^{JIM}_{IJ}\}_i$ corresponding to the column number $i$ of $\tilde{\mathbf{\Phi}}^{JIM}_{IJ}$. The MAC value is bounded between 0 and 1. A MAC value of 1 identifies two highly correlated (or parallel) modes, and a MAC value of 0 corresponds to completely uncorrelated (or orthogonal) modes.

This comparison was performed for the structure indicated in Fig. 5. The jointed structure shown there is fixed at both ends. A thick line indicates the contact area for which the JIMs are computed. Both substructures are connected via a massless beam. The bore hole is neglected.

Table 1 shows the deformation shapes of the first 3 modes of ${}_{\#}\tilde{\mathbf{\Phi}}^{JIM}_{IJ}$ and $\tilde{\mathbf{\Phi}}^{JIM}_{IJ}$. The modes are sorted with respect to increasing

**Table 1 The first 3 modes of ${}_{\#}\tilde{\mathbf{\Phi}}^{JIM}_{IJ}$ and $\tilde{\mathbf{\Phi}}^{JIM}_{IJ}$**

| Mode $i$ | $\{{}_{\#}\varphi^{JIM}_{IJ}\}_i$ | $\{\varphi^{JIM}_{IJ}\}_i$ |
|---|---|---|
| 1 | 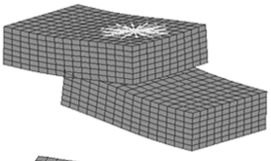 | 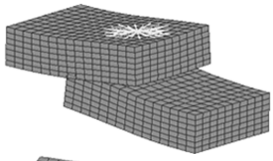 |
| 2 | 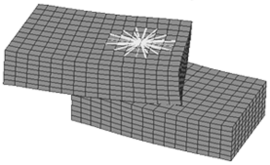 | 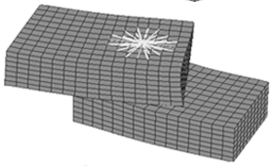 |
| 3 | 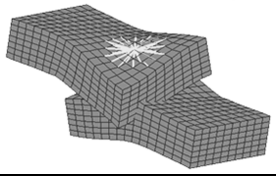 | 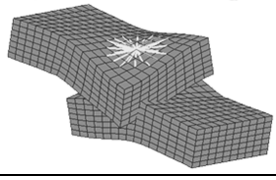 |

eigenvalues according to the eigenvalue problems in Eqs. (25) and (33).

The MAC values of all possible comparisons can be collected in a matrix. The matrix entries $i$ and $j$ represent the MAC value of $\{{}_{\#}\boldsymbol{\varphi}_{\mathrm{IJ}}^{\mathrm{JIM}}\}_i$ and $\{\boldsymbol{\varphi}_{\mathrm{IJ}}^{\mathrm{JIM}}\}_j$. It is obvious that this matrix is symmetric. For the considered example, the MAC matrix is almost an identity matrix. The minimum value of the main diagonal is 0.96. The maximum value of all secondary diagonal entries is 0.13, and the corresponding mean value is 0.002. This indicates that the modes computed by ${}_{\#}\tilde{\boldsymbol{\Phi}}_{\mathrm{IJ}}^{\mathrm{JIM}}$ and $\tilde{\boldsymbol{\Phi}}_{\mathrm{IJ}}^{\mathrm{JIM}}$ are highly correlated (or parallel). This had to be expected, due to the fact that the Guyan reduction is exact in terms of static considerations. The source of the slight difference is the mass matrix used for eigenvalue problems (25) and (33). The mass matrix in eigenvalue problem (33) is a doubly reduced mass matrix, in contrast to the mass matrix in eigenvalue problem (25), which is reduced just once.

Concerning computational efficiency, it can be said that the eigenvalue problems (25) and (33) have the same dimension and complexity. The extension of the JIMs to the entire structure according to Eqs. (26) and (34) is again of the same dimension and complexity. The difference between the two approaches is a practical one and comes into the play when the $(\mathbf{n}_{\mathrm{IJ}}/2 \times \mathbf{n}_{\mathrm{IJ}}/2)$ matrices $\tilde{\mathbf{G}}$ or ${}_{\#}\tilde{\mathbf{G}}$ are to be computed. The computation of ${}_{\#}\tilde{\mathbf{G}}$ requires the inverse of the matrix $\tilde{\mathbf{K}}_{I\setminus\mathrm{IJ},I\setminus\mathrm{IJ}}$, which can be a huge matrix (e.g., up to $10^7$ rows and columns for industrial applications). An efficient computation of ${}_{\#}\tilde{\mathbf{G}}$ in terms of computational time and storage requires optimized software that takes into account the sparse character of the matrix $\tilde{\mathbf{K}}_{I\setminus\mathrm{IJ},I\setminus\mathrm{IJ}}$. The matrix $\tilde{\mathbf{G}}$, in contrast, is based on $(\mathbf{n}_{\mathrm{IJ}} \times \mathbf{n}_{\mathrm{IJ}})$ matrices that are gained by a Guyan [8] reduction of the entire structure to the DOF of $\mathbf{x}_{\mathrm{IJ}}$. The latter Guyan reduction is a typical standard feature of commercially available FE software packages.

Note that the numerical examples that are presented in Sec. IV are performed by using JIMs based on statically reduced mass and stiffness matrices.

### G. Some Brief Remarks on Substructuring

Both introduced methods for the computations of the JIMs are based on the assumption that both contact partners are represented by a single mode base. This is a consequence of the considerations that have been performed in Sec. II. If the jointed structures are not considered in the context of the FFRF or in terms of conventional substructuring, then both substructures are usually represented separately by their own mode base. The idea of the proposed JIMs will then hold, even if slight adaptations of the procedure have to be performed. If the vectors of joint DOF $\mathbf{x}_{\mathrm{IJ1}}$ and $\mathbf{x}_{\mathrm{IJ2}}$ in Eq. (29) are considered as DOF from separate substructures, the coupling matrices $[\tilde{\mathbf{K}}_{\mathrm{red,IJ}}]_{12}$ and $[\tilde{\mathbf{K}}_{\mathrm{red,IJ}}]_{21}$ are consequently zero. The procedure to compute the JIMs can be applied analogously for each substructure. Note that in contrast to conventional substructuring techniques, both involved substructures need to be known for the computation of each mode base.

### H. Short Review of Interface Modes

Following Tran [13], the eigenvalue problem for computing the IMs is based on the matrices $\tilde{\mathbf{K}}_{\mathrm{IJ}}^{\mathrm{red}}$ and $\tilde{\mathbf{M}}_{\mathrm{IJ}}^{\mathrm{red}}$ of Eqs. (27) and (28) and can be written as

$$(\tilde{\mathbf{K}}_{\mathrm{IJ}}^{\mathrm{red}} - (\tilde{\boldsymbol{\Omega}}^{\mathrm{IM}})^2 \tilde{\mathbf{M}}_{\mathrm{IJ}}^{\mathrm{red}})^{*}\tilde{\boldsymbol{\Phi}}_{\mathrm{IJ}}^{\mathrm{IM}} = \tilde{\mathbf{0}} \tag{36}$$

where $\tilde{\boldsymbol{\Omega}}^{\mathrm{IM}}$ is the $(\mathbf{n}_{\mathrm{IJ}} \times \mathbf{n}_{\mathrm{IJ}})$ diagonal matrix of eigenvalues, and ${}^{*}\tilde{\boldsymbol{\Phi}}_{\mathrm{IJ}}^{\mathrm{IM}}$ is the $(\mathbf{n}_{\mathrm{IJ}} \times \mathbf{n}_{\mathrm{IJ}})$ matrix of IMs for all joint DOF $\mathbf{x}_{\mathrm{IJ}}$. Equation (36) has $\mathbf{n}_{\mathrm{IJ}}$ solutions, but a truncated set of eigenvectors $\tilde{\boldsymbol{\Phi}}_{\mathrm{IJ}}^{\mathrm{IM}}$ of the dimension $(\mathbf{n}_{\mathrm{IJ}} \times \mathbf{n}_{\mathrm{IM}})$ will deliver satisfying results $(\mathbf{n}_{\mathrm{IM}} \ll \mathbf{n}_{\mathrm{IJ}})$. The quasi-static extension of the considered modes for $\mathbf{x}_{\mathrm{IJ}}$ to the entire structure takes the form

$$\tilde{\boldsymbol{\Phi}}^{\mathrm{IM}} = \begin{bmatrix} \tilde{\mathbf{0}}^T & [\tilde{\boldsymbol{\Phi}}_{\mathrm{IJ}}^{\mathrm{IM}}]^T & [-\tilde{\mathbf{K}}_{I\setminus\mathrm{IJ},I\setminus\mathrm{IJ}}^{-1}\tilde{\mathbf{K}}_{I\setminus\mathrm{IJ},\mathrm{IJ}}\tilde{\boldsymbol{\Phi}}_{\mathrm{IJ}}^{\mathrm{IM}}]^T \end{bmatrix}^T \tag{37}$$

where $\tilde{\boldsymbol{\Phi}}^{\mathrm{IM}}$ is a $(\mathbf{n} \times \mathbf{n}_{\mathrm{IM}})$ matrix. If IMs instead of JIMs are used, the modal transformation takes the form

$$\mathbf{x} \cong \tilde{\boldsymbol{\Phi}}\mathbf{q} = \begin{bmatrix} \tilde{\boldsymbol{\Phi}}^{\mathrm{classical}} & \tilde{\boldsymbol{\Phi}}^{\mathrm{IM}} \end{bmatrix}\mathbf{q} \tag{38}$$

It is to be expected that the presented modes represented by $\tilde{\boldsymbol{\Phi}}^{\mathrm{JIM}}$ converge faster to an accurate solution than those provided by $\tilde{\boldsymbol{\Phi}}^{\mathrm{IM}}$, because in the present new formulation, we have explicitly taken into account the principle of action equal to reaction (or Newton's third law) in the joint. A numerical confirmation of this assumption will be given next.

## IV. Numerical Examples

In this section, static and dynamic examples are presented to outline the benefits and the potential of the proposed JIMs approach. The FE computations have been performed with the commercially available code MSC.NASTRAN [22]; for the mode-based computations, the commercially available software package MSC.ADAMS [23] has been used. The computation of the JIMs based on Guyan-type reduced matrices has been performed with the freely available software Scilab [24]. For the subsequent examples, the CPU time for the computation of the JIMs was in the range of several minutes. However, for industrial applications, the entire CPU time of the proposed procedure is dominated by the Guyan [8] reduction, which is known to be very expensive for huge structures and large interfaces. In future work, possibilities for decreasing this CPU time will be discussed.

Because of the choice of the software packages, it is advantageous to use the Craig–Bampton [10] mode base, which is extended by JIMs and IMs in the following examples. Consequently, from now on, the general matrix $\tilde{\boldsymbol{\Phi}}^{\mathrm{classical}}$ is denoted as $\tilde{\boldsymbol{\Phi}}^{\mathrm{CB\text{-}CMS}}$, such that the transformation rule (18) takes the more specific form

$$\mathbf{x} \cong \tilde{\boldsymbol{\Phi}}\mathbf{q} = \begin{bmatrix} \tilde{\boldsymbol{\Phi}}^{\mathrm{CB\text{-}CMS}} & \tilde{\boldsymbol{\Phi}}^{\mathrm{JIM}} \end{bmatrix}\mathbf{q} \quad \text{or}$$

$$\mathbf{x} \cong \tilde{\boldsymbol{\Phi}}\mathbf{q} = \begin{bmatrix} \tilde{\boldsymbol{\Phi}}^{\mathrm{CB\text{-}CMS}} & \tilde{\boldsymbol{\Phi}}^{\mathrm{IM}} \end{bmatrix}\mathbf{q}$$

For the sake of brevity, a nonlinear penalty-contact (soft-contact) model has been implemented for the numerical investigations presented subsequently as a simple constitutive model of the interface. Note that the focus of our contribution is on the capability of the JIMs to approximate the joint state and not on the contact model itself. The joint area is modeled with two free congruent FE surfaces and with FE node pairs, which are coincident in the reference position. Moreover, it is assumed that the relative displacements of the involved contact surfaces are small. For the FE node pair number $j$ that belongs to the joint, the normal and tangential contact forces are given as

$${}^{\mathrm{IJ}}\mathbf{f}_j^{\mathrm{normal}} = \begin{cases} 0 & \Delta^{\mathrm{IJ}}\mathbf{x}_j^{\mathrm{normal}} \geq 0 \\ \mathbf{k}^{\mathrm{normal}}\Delta^{\mathrm{IJ}}\mathbf{x}_j^{\mathrm{normal}} & \Delta^{\mathrm{IJ}}\mathbf{x}_j^{\mathrm{normal}} < 0 \end{cases}$$

$${}^{\mathrm{IJ}}\mathbf{f}_j^{\mathrm{tangential}} = \begin{cases} 0 & \Delta^{\mathrm{IJ}}\mathbf{x}_{\mathrm{j}}^{\mathrm{normal}} \geq 0 \\ \mathbf{k}^{\mathrm{tangential}}\Delta^{\mathrm{IJ}}\mathbf{x}_{\mathrm{j}}^{\mathrm{tangential}} + \mathbf{d}\Delta^{\mathrm{IJ}}\dot{\mathbf{x}}_j^{\mathrm{tangential}} & \Delta^{\mathrm{IJ}}\mathbf{x}_{\mathrm{j}}^{\mathrm{normal}} < 0 \end{cases} \tag{39}$$

where ${}^{\mathrm{IJ}}\mathbf{f}_j$ represents the contact force acting on FE node pair number $j$ expressed in joint fixed coordinates. The symbols $\Delta^{\mathrm{IJ}}\mathbf{x}_j$ and $\Delta^{\mathrm{IJ}}\dot{\mathbf{x}}_j$ denote the relative displacements and velocities of FE node pair number $j$ with respect to joint fixed coordinates. If $\Delta^{\mathrm{IJ}}\mathbf{x}_j^{\mathrm{normal}}$ is negative, the contact is closed; otherwise, the contact surfaces are gapping. The penalty stiffness in the normal and tangential directions of the contact surfaces are $\mathbf{k}^{\mathrm{normal}}$ and $\mathbf{k}^{\mathrm{tangential}}$, respectively. For the dynamic analysis, a viscous damping is taken into account that is characterized by the damping coefficient $d$. The collection of all forces that act on the $\mathbf{n}_{\mathrm{IJ}}/2$ FE node pairs of the joint gives the force vector in Eqs. (20) and (29) with respect to a joint fixed coordinate system.

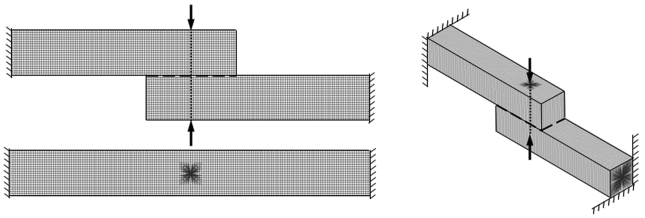

**Fig. 6 Front, top, and 3-D views of a double-sided clamped cantilever beam with a preloaded bolt.**

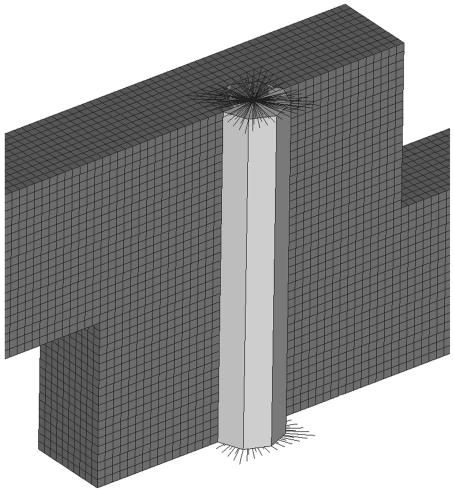

**Fig. 7 Detail of the bolt (cut along the structure's midplane).**

Note that other, more complex, contact and friction models (such as Coulomb friction) could be implemented as well. The JIM mode base itself is independent of the selected contact model.

### A. Simple Joint: Static Example

A static simulation of a double-sided clamped beam, which is indicated in Fig. 6, was performed. The FE model consists of two identical substructures that are connected via a bolt, represented by a massless beam. The bolt is indicated by a dotted line in Fig. 6. The bore hole is neglected. Note that the bolt itself is part of the FE model and it is connected via a constraint to the nodes on the corresponding solid surface, as indicated in Fig. 7. This is a common FE modeling approach when the contact between the bolt nut and the structure is neglected. Each substructure has a length of 100 mm and a cross section of 20 by 20 mm. The contact surface, which is indicated by a dashed line in Fig. 6, is of the dimension 40 by 20 mm. The DOF of these FE nodes correspond to $\mathbf{x}_{\mathrm{IJ}}$. For the support, two interface nodes in the middle of a rigid plane are determined: one at each end of the whole structure. Note that these DOF are represented by the vector $\mathbf{x}_B$. The material parameters have been chosen according to iron.

For the classical Craig–Bampton mode base $\tilde{\mathbf{\Phi}}^{\mathrm{CB\text{-}CMS}}$, 12 constraint modes due to $\mathbf{x}_B$ are considered, together with 10 fixed-boundary normal modes and one load vector caused by the bolt load. For more details on the latter-mentioned modes, refer to [3,4]. To compare the convergence rate, the classical Craig–Bampton mode base $\tilde{\mathbf{\Phi}}^{\mathrm{CB\text{-}CMS}}$ is extended by interface modes $\tilde{\mathbf{\Phi}}^{\mathrm{IM}}$ and the proposed joint interface modes $\tilde{\mathbf{\Phi}}^{\mathrm{JIM}}$.

First, an $h$-convergence study has been performed to ensure a valid element size. The final FE model has 534,516 DOF using linear solid elements of the MSC.NASTRAN code. The modes have been computed with MSC.NASTRAN and have been imported into the multibody system (MBS) code MSC.ADAMS, in which the mode-based computations has been performed. In the MBS, both interface nodes have been fixed with respect to ground. The bolt was preloaded with 18 kN, which is indicated in Fig. 6 by two arrows. A penalty-contact model according to Eq. (39) has been used. The normal and tangential contact stiffnesses have been set to $10^5$ and $10^4$ N/mm, respectively. As a reference solution, a nonlinear FE computation with all nodal DOF and the same contact model was performed using the MSC.NASTRAN solver.

A quantity for the error between the reference solution (left superscript $r$) and the mode-based computation (left superscript $m$) is given by

$$\alpha_p = \left( \frac{\| {}^m\boldsymbol{\sigma}_{\mathrm{IJ}}^{\mathrm{VM}} \|_p}{\| {}^r\boldsymbol{\sigma}_{\mathrm{IJ}}^{\mathrm{VM}} \|_p} - 1 \right) 100 \tag{40}$$

where $\| \ \|_p$ indicates the $p$-norm of the vector $\boldsymbol{\sigma}_{\mathrm{IJ}}^{\mathrm{VM}}$, which denotes the von Mises stress at the FE nodes corresponding to the vector $\mathbf{x}_{\mathrm{IJ}}$. The stresses are interpolated from the FE element Gauss point to the FE nodes by the FE code MSC.NASTRAN.

In a series of computations, the relative errors of the Manhattan norm ($p = 1$), the Euclidian norm ($p = 2$), and the maximum norm ($p = \infty$) are evaluated. A summary of the computations done with IMs and JIMs can be seen in Figs. 8–10, which lead to the following conclusions:

1) Both mode bases converge with increasing the number of modes to the reference solution.

2) Even for this simple joint geometry, the JIMs $\tilde{\mathbf{\Phi}}^{\mathrm{JIM}}$ converge much faster than the interface modes $\tilde{\mathbf{\Phi}}^{\mathrm{IM}}$. In the case of the considered example, just 25 additional joint interface modes deliver stresses with acceptable accuracy. To obtain a comparable result with interface modes, at least 4 times as many modes are necessary.

3) An insufficient number of $\tilde{\mathbf{\Phi}}^{\mathrm{JIM}}$ and $\tilde{\mathbf{\Phi}}^{\mathrm{IM}}$ or neglecting them entirely will lead to inaccurate results.

A practical consequence of the faster convergence of JIMs with respect to IMs is a reduced number of DOF and consequently a reduced computational effort for results with the same accuracy.

### B. Complex Joint: Dynamic Example

In a next step, a dynamic example with a more complex joint geometry is considered. The FE model shown in Fig. 11 represents a steel box that consists of a body and a cap. The outer dimension of the body is $82.5 \times 82.5 \times 100$ mm with a wall thickness of 17.5 mm.

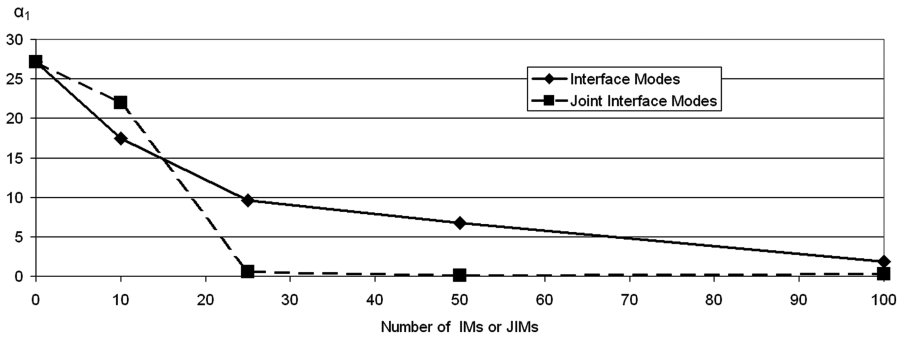


**Fig. 8 Relative error (%) $\alpha_1$ of the Manhattan norm ($p = 1$) of the von Mises stress vector across the joint.**

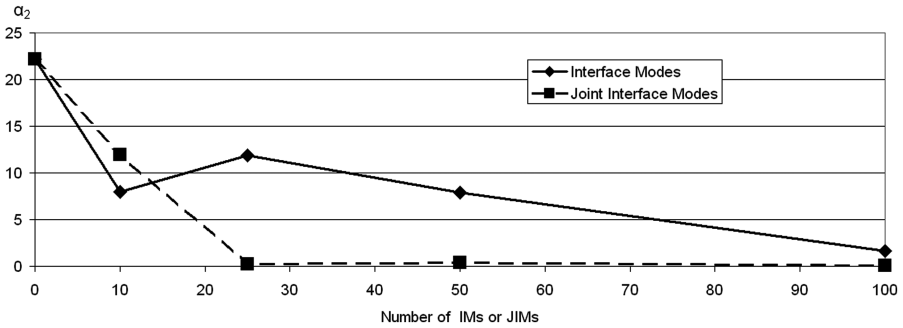


**Fig. 9 Relative error (%) $\alpha_2$ of the Euclidian norm ($p = 2$) of the von Mises stress vector across the joint.**

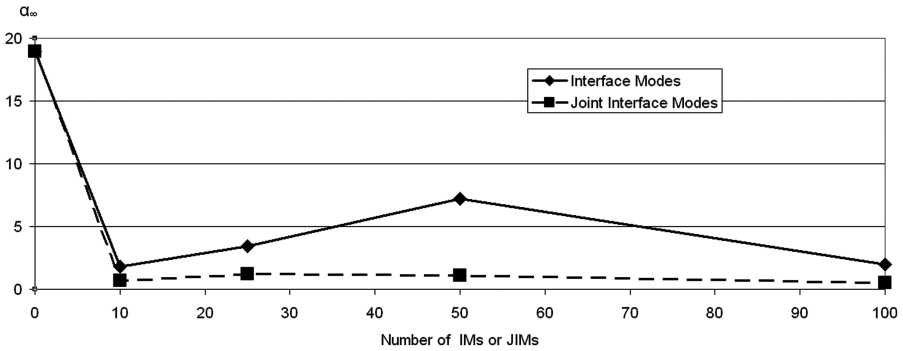


**Fig. 10 Relative error (%) $\alpha_\infty$ of the maximum norm ($p = \infty$) of the von Mises stress vector across the joint.**

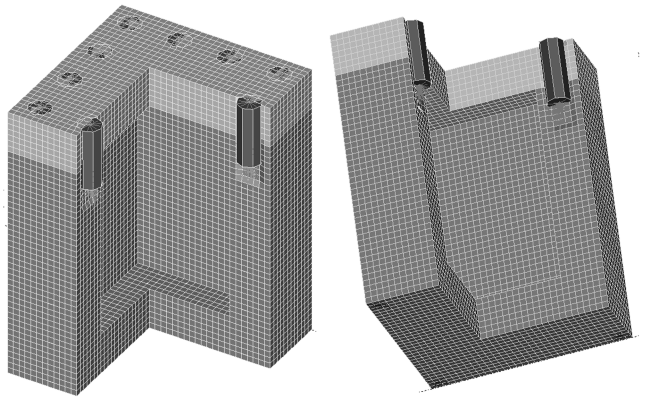

**Fig. 11 FE model of the box with a bolted cap.**

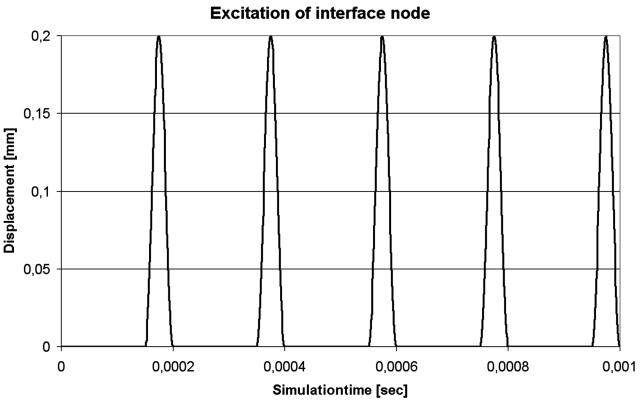


**Fig. 13 Time characteristic of excitation.**

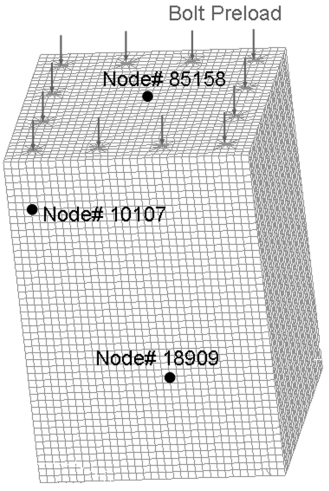


**Fig. 12 Locations of bolt preload and evaluated nodes.**

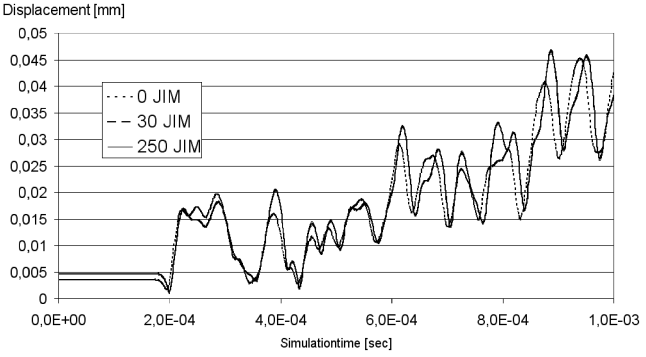


**Fig. 14 Displacement magnitude of node 85188.**

The dimension of the cap is $82.5 \times 82.5 \times 17.5$ mm. The cap is mounted on the body by 12 screws. The screws are modeled as massless beams with a diameter of 10 mm. The bolts are attached to the underlying solid structure in a manner similar to that indicated in Sec. IV.A. The bores are neglected. On the bottom of the body, 4

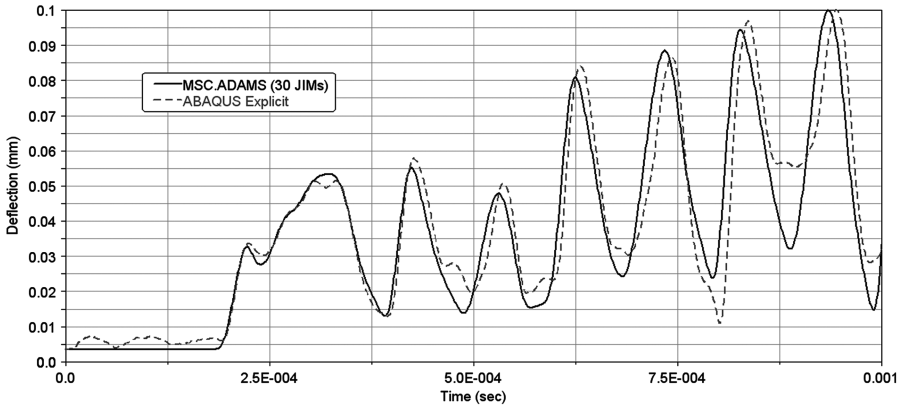


**Fig. 15 Deflection magnitude of node 85158 computed with ABAQUS Explicit and MSC.ADAMS using 30 JIMs.**

nodes for the mounting and excitation are modeled. These nodes are called *interface nodes* and the corresponding DOF are represented by the vector $\mathbf{x}_B$ in Sec. III.A.

An *h*-convergence analysis was performed to ensure that proper-sized linear solid elements are used. It turned out that a global FE element edge length of 2.5 mm delivers results of satisfying accuracy. For the CMS, 100 fixed-boundary normal modes are considered. This spans a frequency range up to approximately 50,000 Hz.

In the mode-based multibody simulation in MSC.ADAMS, three interface nodes are mounted with linear springs in the $x$, $y$, and $z$ directions to ground. The bolts are preloaded with 20 kN, and the remaining interface point is excited by an imposed deformation. The load is represented by a series of deflection impulses, with one period having a frequency of 5000 Hz. The time characteristic of the load can be seen in Fig. 13. The joint is modeled according to Eq. (39), with $10^5$ N/mm normal stiffness, $10^4$ N/mm tangential stiffness, and a tangential damping coefficient of 1 Ns/mm.

During the multibody simulation, no global modal damping is considered. The integration has been performed with the Hilber–Hughes–Taylor integrator of MSC.ADAMS (Negrut et al. [25]), using a step size of $1.0e-7$. The simulation endured 0.001 s and was performed with a maximum local error of $1.0e-7$. Several tests have been performed to ensure that the step size and error are small enough to obtain a converged solution.

Table 2 shows the converged magnified deformation in the area of the joint at two arbitrary time steps. The figures indicate that several modes are necessary to approximate the deformation state, which was the intention of the considered example. The joint is partially gapping, which leads to nonlinearities in the system.

The displacement magnitudes of three different FE nodes with respect to the initial position have been evaluated. The selected nodes have the labels 10107, 85158, and 18909 and are indicated in Fig. 12. Because of the fact that the results of all three nodes have the same characteristics, just the result of node 85158 will be presented here. Figure 14 contains the displacement magnitude of node 85158 for a computation with no additional JIM, a computation with 30 additional JIMs, and a computation with 250 additional JIMs, which is considered as the reference computation. It can be seen that just 30 additional JIMs will increase the quality of the result significantly, even though the Craig–Bampton mode base already has a considerable dimension.

**Table 2 Screen shot of the magnified deformation in the joint area at two arbitrary time steps**

| Simulation time | Deformation (magnified by a factor of 750) |
|---|---|
| 6e-4 | 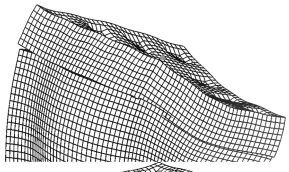 |
| 8e-4 | 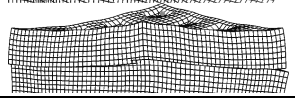 |

The conclusions drawn from Fig. 14 are as follows:

1) An insufficient number of JIMs or neglecting them entirely will lead to remarkable errors.

2) The solution converges with an increasing number of JIMs.

3) Just 30 additional JIMs are necessary to obtain a solution with a negligible error.

Because the superior convergence of the JIMs with respect to the IMs has been demonstrated in the preceding section, an additional comparison of JIMs and IMs has not been performed.

The state-of-the-art alternative to using JIMs would be the use of a direct nonlinear FE solver. Such a comparison has been performed with the explicit solver of ABAQUS [26]. For the sake of comparison, the tangential contact forces have been set to zero. For the mode base simulations with MSC.ADAMS, 30 JIMs have been considered. The deflection magnitude of node 85158 can be seen in Fig. 15.

Two remarks can be made concerning the differences: First, it should be considered that ABAQUS Explicit is an explicit formulation. Second, it is worth mentioning that ABAQUS Explicit supports a penalty contact that is slightly different from that introduced in Eq. (39). The benefit of the JIM formulation can be seen by considering the simulation time, which was 645 s in the case of the ABAQUS simulation and 61 s in the case of the mode-based simulation with MSC.ADAMS using JIMs.

## V. Conclusions

The proposed joint interface modes represent an effective extension of existing mode bases for the time integration of huge and complex FE structures that contain joints. Joint interface modes provide the ability to do an effective mode-based time integration of jointed structures with an accuracy that was, up to now, subject to direct, node-based, and thus necessarily very costly FE computations. In the presented numerical examples, a fast convergence has been observed when using the proposed joint interface modes.

## Acknowledgments

Support of this work in the framework of Kplus, Linz, Austria, is gratefully acknowledged. This work has been performed as a part of the Linz Center of Competence in Mechatronics, Austria, project no. 140200, with the partner company Engineering Center Steyr, Magna Powertrain, Austria. The authors particularly appreciate the interest and valuable remarks by Bernhard Unger, Helmut Dannbauer, and Harald Riener.

## References


[1] Gaul, L., and Nitsche, R., "The Role of Friction in Mechanical Joints," *Applied Mechanics Reviews*, Vol. 54, No. 2, 2001, pp. 93–105.

[2] Noor, A. K., "Recent Advances and Applications of Reduction Methods," *Applied Mechanics Reviews*, Vol. 47, No. 5, 1994, pp. 125–146.

[3] Craig R. J., "Coupling of Substructures for Dynamic Analyses: An Overview," 41st AIAA/ASME/ASCE/AHS/ASC Structures, Structural Dynamics, and Materials Conference and Exhibit, Atlanta, GA, AIAA Paper 2000-1573, 2000.

[4] Craig R. J., "A Review of Time-Domain and Frequency-Domain Component Mode Synthesis Methods," *The International Journal of Analytical and Experimental Modal Analysis*, Vol. 2, No. 2, 1987, pp. 59–72.

[5] Meirovitch, L., *Computational Methods in Structural Dynamics*, Sijthoff & Noordhoff, Alphen Aan Den Rijn, The Netherlands, 1980.

[6] Zu, Q. Q., *Model Order Reduction Techniques*, Springer–Verlag, London, 2004.

[7] Koutsovasilis, P., and Beitelschmidt, M., "Model Reduction of Large Elastic Systems–A Comparison Study on the Elastic Piston Rod," *Proceedings of the 12th IFToMM World Congress* [online proceedings], edited by J.-P. Merlet, and M. Dahan, 2007, http://130.15.85.212/proceedings/WorldCongress07/articles/sessions/papers/A391.pdf [retrieved 3 Sept. 2008].

[8] Guyan R. J., "Reduction of Stiffness and Mass Matrix," *AIAA Journal*, Vol. 3, No. 2, 1965, pp. 380.
doi:10.2514/3.2874

[9] Hurty W. C., "Dynamic Analysis of Structural Systems Using Component Modes," *AIAA Journal*, Vol. 3, No. 4, 1965, pp. 678–685.
doi:10.2514/3.2947

[10] Craig R. R., and Bampton M. C. C., "Coupling of Substructures for Dynamic Analysis," *AIAA Journal*, Vol. 6, No. 7, 1968, pp. 1313–1319.
doi:10.2514/3.4741

[11] Craig R. R., Jr., and Tzu-Jen, Su, "Krylov Model Reduction Algorithm for Undamped Structural Dynamics Systems," *Journal of Guidance, Control, and Dynamics*, Vol. 14, No. 6, 1991, pp. 1311–1313.
doi:10.2514/3.20789

[12] Castanier M. P., Tan Yung-Chan, and Pierre, C., "Characteristic Constraint Modes for Component Mode Synthesis," *AIAA Journal*, Vol. 39, No. 6, 2001, pp. 1182–1187.
doi:10.2514/2.1433

[13] Tran, D. M., "Component Mode Synthesis Methods Using Interface Modes. Application to Structures with Cyclic Symmetry," *Computers and Structures*, Vol. 79, 2001, pp. 209–222.
doi:10.1016/S0045-7949(00)00121-8

[14] Farhat, C., and Geradin, M., "A Hybrid Formulation of a Component Mode Synthesis Method," AIAA Paper 92-2383, 1992, pp 1783–1796.

[15] Balmes, E., "Use of Generalized Interface Degrees of Freedom in Component Mode Synthesis," *Proceedings of the 14th International Modal Analysis Conference*, Society of Experimental Mechanics, Bethel, CT, 1996; also available at http://www.sdtools.com/pdf/IMAC96int.pdf [retrieved 3 Sept. 2008].

[16] Muravyov, A., and Hutton, S. G., "Component Mode Synthesis for Nonclassically Damped Systems," *AIAA Journal*, Vol. 34, No. 8, 1996, pp. 1664–1669.
doi:10.2514/3.13287

[17] Rosenberg, R. M., "On Nonlinear Vibrations of Systems with Many Degrees of Freedom," *Advances in Applied Mechanics*, Vol. 9, 1966, pp. 155–242.

[18] Shabana, A., *Dynamics of Multibody Systems*, 3rd ed., Cambridge Univ. Press, Cambridge, MA, 2005.

[19] Witteveen, W., and Irschik, H., "Efficient Modal Formulation for Vibration Analysis of Solid Structures with Bolted Joints," 25th International Modal Analysis Conference (IMAC XXV), Society of Experimental Mechanics, Paper 385, 2007.

[20] Laursen, A. T., *Computational Contact and Impact Mechanics*, Springer–Verlag, Berlin, 2002, p. 76.

[21] Allemang, R. J., and Brown, D. L., "A Correlation Coefficient for Modal Vector Analysis," *Proceedings of the 1st International Modal Analysis Conference (IMAC I)*, Society of Experimental Mechanics, Bethel, CT, 1982, pp. 110–116.

[22] MSC.NASTRAN, Software Package, Ver. 2005, MSC Software Corp., Santa Ana, CA, 2005.

[23] MSC.ADAMS, Software Package, Ver. 2007r2, MSC Software Corp., Santa Ana, CA, 2007.

[24] Scilab, Software Package, Ver. 4.1.2, Inst. National de Recherche en Informatique et en Automatique, Paris, 2007.

[25] Negrut, D., Ottarsson, G., Rampalli, R., and Sajdak, A., "On an Implementation of the Hilber-Hughes-Taylor Method in the Context of Index 3 Differential-Algebraic Equations of Multibody," *Journal of Computational and Nonlinear Dynamics*, Vol. 2, No. 1, Jan. 2007, pp. 73–85.
doi:10.1115/1.2389231

[26] ABAQUS, Software Package, Ver. 6.7.1, SIMULIA, Providence, RI, 2007.


A. Palazotto
*Associate Editor*